# Effects of Cr-to-Al ratio on the oxidation behaviour of CoNiCrAl alloys

By Yusheng Zong (20615602)

Supervisor: Dr. Hao Chen

Dr. Adam Rushworth

A master thesis submitted to the University of Nottingham, for the degree of Master of Research in Material Science and Engineering

Department of Mechanical, Materials, and Manufacturing Engineering

October 2024

# Preface

This thesis is submitted to the University of Nottingham, Ningbo, China for the degree of Master of Research in Material Science and Engineering. The research was carried out under the supervision of Dr. Hao Chen and Dr. Adam Rushworth in the Faculty of Science and Engineering.

It is certified that the work presented in this thesis is original, or proper references are made for any work cited from the literature.

# Abstract

This thesis studies the effects of chromium to aluminium atomic ratio (Cr-to-Al ratio) on the microstructure evolution and oxidation mechanisms of as-cast CoNiCrAl alloys at 1100 °C. CoNiCrAl alloys serve as bond coat materials in thermal barrier coatings systems and are classified as high entropy alloys (HEAs). Due to their outstanding chemical and mechanical performance, they have been widely used as protective coating materials. To focus specifically on the Cr-to-Al ratio, the weight percentages of cobalt and nickel were held constant, as 39.4% Ni and 31.7% Co throughout this study. As-cast CoNiCrAl alloys with five different Cr-to-Al ratios were prepared by the vacuum arc melting and casting process. High temperature oxidation tests were conducted at 1100 °C in air at time intervals of 2 h, 10 h, 25 h, 50 h and 100h. Prior to the oxidation tests, an initial vacuum heat treatment was carried out to the as-cast CoNiCrAl alloys for microstructure homogenisation.

The results showed that the Cr-to-Al ratio significantly influenced the formation of competing oxides, $Cr_2O_3$ and $Al_2O_3$. A critical threshold at Cr-to-Al ratio of approximately 1.8 was proposed. Below the threshold, an exclusive $Al_2O_3$ layer was formed, whereas, above the threshold, the formation of outer layer $Cr_2O_3$ was allowed by outward diffusion of Cr in the low Al content CoNiCrAl alloy through incomplete $Al_2O_3$ layers. Notably, this threshold decreased with increasing oxidation time.

# Acknowledgement

I would like to deliver my sincere appreciation to all the individuals and departments that supported me throughout the research process at the beginning of this thesis.

First and foremost, I am deeply grateful to my supervisor, Prof. Hao Chen. His systematic guidance through the research process was invaluable. He helped clarify the details I needed to focus on, ensuring that I recorded and verified my findings accurately. With his profound academic insight and extensive research experience, he not only helped me elevate my work to a level suitable for publication but also pointed out my misunderstandings and clarified my confusions. Without his support, I would not have developed into a competent researcher, and my efforts could have been wasted.

Secondly, I would also like to thank lab supervisor John Zhu, whose assistance with instrument operation and maintenance, safety guarantee, and consumable replenishment. He was crucial in keeping my experiments on schedule.

Additionally, I am grateful to the staff of FOSE and CBI for their timely instrument training and technical support, including help with SEM and XRD, etc. Their precise assistance was essential to the success of my study. Thanks to my colleague, Liangyi Sun, for her collaboration, helped me from the emergencies.

Finally, I wish to express my deepest gratitude to my family, who have been my backbone, providing support and understanding that allowed me to concentrate on my research.

Without the contributions of all these individuals, completing this thesis would have been impossible. Thank you to everyone who has helped me along this study.

# List of Tables

# List of Figures

# Abbreviations

**HEA** High entropy alloy

**TBC** Thermal barrier coating

**SEM** Scanning electron microscopy

**EDS** energy-dispersive spectroscopy

**XRD** X-ray diffraction

**FCC** Face-centred cubic

**BCC** Body-centred cubic

**VAM** Vacuum arc melting

**HT** Heat-treated

# Table of Content

# Chapter 1 Introduction

## 1.1 Background

To meet continuous demands of turbine engine efficiency and to withstand the harsh operating environments in gas turbine engines [1-4], materials with high temperature stability and excellent oxidation resistance are of great interest. MCrAlY alloy (M=Ni/Co or a mixture of both), recognised as a novel material of transition metal high entropy alloy, is capable of providing thermal protection and prolonging service life of substrate material, due to its outstanding chemical and thermal stability [5, 6]. Thus, it has been widely used as a bond coat alloy in thermal barrier coating systems. Although the microstructure and oxidation characteristics of MCrAlY alloys have been widely studied [7, 8], existing research predominantly limited to the commercially available compositions. These commercial MCrAlY materials are facing challenges in meeting the rising demands of higher turbine inlet temperatures due to the degradation caused by inter-diffusion between coatings and substrates [9]. Therefore, development of novel MCrAlY with promising microstructure, phase stability and anti-oxidation performance is necessary to tackle these challenges.

MCrAlY alloys typically exhibit a multi-phase structure, including face-centred cubic (fcc) γ/γ’ phase (rich in Ni or Co), and intermetallic body-centred cubic (bcc) β (rich in Al) phase [10, 11]. It is believed that the bcc-β phase is responsible for the outstanding oxidation resistance of MCrAlYs, acting as an aluminium reservoir that facilitates the formation of α-$Al_2O_3$, which serves as a protective oxide scale [12, 13].

To achieve a sufficient concentration of the β phase, it is essential to incorporate adequate aluminium in the MCrAlY composition. Previous studies primarily focus on the oxide growth

mechanisms using the commercial MCrAlY powder compositions [14], often modifying the microstructure by adjusting aluminium content. However, simply rising Al content is not practical. Excessive content of aluminium can lead to the formation of the detrimental σ phase, which negatively impacts performance of the alloy due to the aggregation of cobalt and chromium [15]. Additionally, stable $Cr_2O_3$ can form at elevated temperatures as a secondary protective oxide from the fcc-γ phase [16].

While it is widely recognised that a dense alumina scale can form on the MCrAlY alloy surface, a dual-layer oxide structure consisting of an outer layer of spinel oxides (which is in the form of $(Ni,Co)(Al,Cr)_2O_4$ in this study) and an inner layer of alumina has also been observed, depending on the heat treatment history [17, 18]. Thus, investigating the thermodynamic phase equilibria and oxidation behaviour of MCrAlY alloys with varying chromium-to-aluminium (Cr-to-Al) ratios is critical to revealing the competing growth mechanisms of $Cr_2O_3$ and $Al_2O_3$ during oxidation. Since stable $Cr_2O_3$ can also form during the high temperature exposure, it is the Cr-to-Al ratio which account for oxidation and hot corrosion resistance, which is a key to extending the service life of MCrAlY materials. Notably, previous studies have not thoroughly explored the effects of Cr-to-Al ratios and the corresponding competing oxide growth mechanisms.

This study aims to evaluate the microstructure evolution of CoNiCrAl bond coat alloys, focusing on the influence of Cr-to-Al ratio on phase transitions under severe high temperature conditions. Yttrium is excluded from this study, as its inclusion in MCrAlY alloys is typically not substantial enough to significantly alter phase equilibria.

In summary, the primary objective of this thesis is to reveal the competing oxide growth

mechanisms of $Cr_2O_3$ and $Al_2O_3$ at various Cr-to-Al ratios in CoNiCrAl alloys and to explore new compositional and microstructure design of MCrAlY high entropy alloys. The vacuum arc melting (VAM) and casting method is employed to cast CoNiCrAl alloys. The oxidation evolution of CoNiCrAl alloys of various Cr-to-Al ratios, subjected to heat treatment at 1300°C (as indicated by previously work published in a wide range of heat treatment attempts [19]) was analysed by X-ray diffraction (XRD) and scanning electron microscopy (SEM). Additionally, the elemental composition of phases was qualitatively analysed via energy dispersive spectroscopy (EDS), and the phase distributions were further quantified using ImageJ software [20].

### 1.2 Project objectives and thesis structure

This thesis mainly focuses on the microstructure evolution of CoNiCrAl alloys in the oxidation process, to reveal the competing oxide growth mechanism at different Cr-to-Al ratios. The main objectives of this research include:

- Understand how the Cr-to-Al ratio impacts the alloys by identifying compositions of each CoNiCrAl alloys in different stages (as-cast state, heat treated state and oxidised state).
- Reveal the mechanism of competing oxide growth between $Cr_2O_3$ and $Al_2O_3$ By characterising the microstructure evolution of the alloys in the oxidation process.
- Provide a prediction method for the oxide growth by analysing the effects of the Cr-to-Al ratio on the oxide growth behaviour of CoNiCrAl alloys theoretically.

The outline of the thesis is as follows:

Chapter 2: Literature review provides a comprehensive review of bond coat high-entropy

alloys (HEAs), the vacuum arc melting method, and the heat treatment processes. It defines each topic, discusses their applications, outlines practical methodologies, and identifies gaps in the existing literature.

Chapter 3: Methodology illustrates the experiment procedures employed in this study, outlining the objectives of each step while emphasizing the expected design outcomes.

Chapter 4: Results and discussion represents the experimental results, and characterises and theoretically analyses them to further explore the potential oxidation mechanisms.

Chapter 5: Conclusion summarises the main outcome of the research, highlighting key findings and contributions.

Chapter 6: Future work discusses potential gaps related to the study, along with schedules for future experiments to address these gaps.

# Chapter 2 Literature review

## 2.1 Bond coat alloys

### 2.1.1 Background

Bond coat alloys are defined as alloys used between thermal barrier coatings (TBCs) and substrates, providing thermal protection, enhancing extremely high temperature performance, and prolonging service life [21]. They are particularly popular in high temperature applications as gas turbines and aerospace components. Common bond coat alloys are MCrAlY and Pt-modified aluminides, with additives of Ce, Y, Cr, Pd, Pt, Rh, Hf and Ir [22]. These alloys serve as intermediate layers between the inner substrate and the outer thermal barrier coatings, with functions of adhesion facilitation, oxidation and corrosion resistance enhancement, thermal stress and conductivity adjustment [23].

The primary function of bond coat alloys is improving the adhesion between the substrate and the thermal barrier coating. A practical bond coat is able to create a strong interfacial bond that can withstand the thermal and mechanical stresses applied by extreme temperatures. This is especially important in applications subjected to thermal cycling, where diverse expansion and contraction can lead to destruction of the layers.

Another critical application of bond coat alloys is to resist oxidation and corrosion at elevated temperatures. They often form protective oxide layers that seal the underlying substrate from environmental exposure. The formation of these layers is critical for extending the service life of TBCs, particularly in combustion environments characterised by presence of high temperatures and reactive contaminants.

Bond coat alloys are also designed for their capable mechanical and microstructure stabilities

at high temperature. Thermal stability of bond coat is essential to ensure that the component functions correctly throughout its service time. High melting points and excellent thermal stabilities are desirable attributes for effective bond coat alloys.

Additionally, bond coats adjust the thermal conductivity and stress within the coating system. In short-term protection, some bond coats may provide lower thermal conductivity to reduce heat transfer to the substrate, thereby enhancing the effectiveness of the thermal barrier coating system. In long-term thermal cycling, effective bond coats can help mitigate a significant degree of stresses arising from differences in thermal expansion coefficients between the bond coat and the substrate, reducing the risk of cracking or delaminating in the thermal barrier system.

In conclusion, high-quality bond coat alloys are essential for meeting the demands of adhesion facilitation, enhancing oxidation and corrosion resistance, and managing thermal stress and conductivity in components designed for high-temperature applications. These alloys play a crucial role in ensuring the durability and performance of thermal barrier coating systems.

### 2.1.2 High entropy alloys

Bond coat alloys, which are required to maintain high durability and stability at elevated temperatures, are satisfied by high-entropy alloys (HEAs), a novel class of protective coating materials. The distinctive composition of HEAs contributes to their unique microstructures and performance characteristics.

Unlike traditional alloys, which typically consist of one or two primary metals supplemented with minor additions, HEAs are defined as mixtures of five or more principal elements in

approximate proportions [24]. This distinctive composition contributes to their unique properties and performance characteristics.

One of the defining features, the most distinguishing feature of HEAs is their intrinsic attribution of high mixing entropy, which exceeds 1.5R (where R = 8.314 J/mol/K), compared to the lower entropy values found in traditional alloys (<R) [25]. The high configuration entropy results in a relatively low Gibbs free energy, contributing to the inherent chemical stability of HEAs. Consequently, this stability allows HEAs to demonstrate unpredictable but superior performance, characterised by complex microstructures that differentiate them from traditional alloys.

HEAs can be categorised based on their principal elements into several types, including transition metal HEAs, refractory metal HEAs, light metal HEAs and etc. For some compositions of HEAs, HEAs are allowed to be comprehensively and exceptionally stable, staying stiff, tough and ductile while holding strong resistances of oxidation and wear though it is expected to be brittle due to its complex microstructures according to traditional alloy design empirical formulas. Each category of HEA offers specific advantages in terms of mechanical strength, thermal stability, and density. **Figure 2-1** displays strength and density ranges of lightweight HEAs (LW-HEAs), which commonly have a density less than $6g/m^3$, and conventional alloys [26]. Notably, HEA is capable to achieve a doubled strength level compared to aluminium while maintaining a lower density. The impressive performance of HEAs can mainly be attributed to 3 primary mechanisms, as detailed below [26, 27].

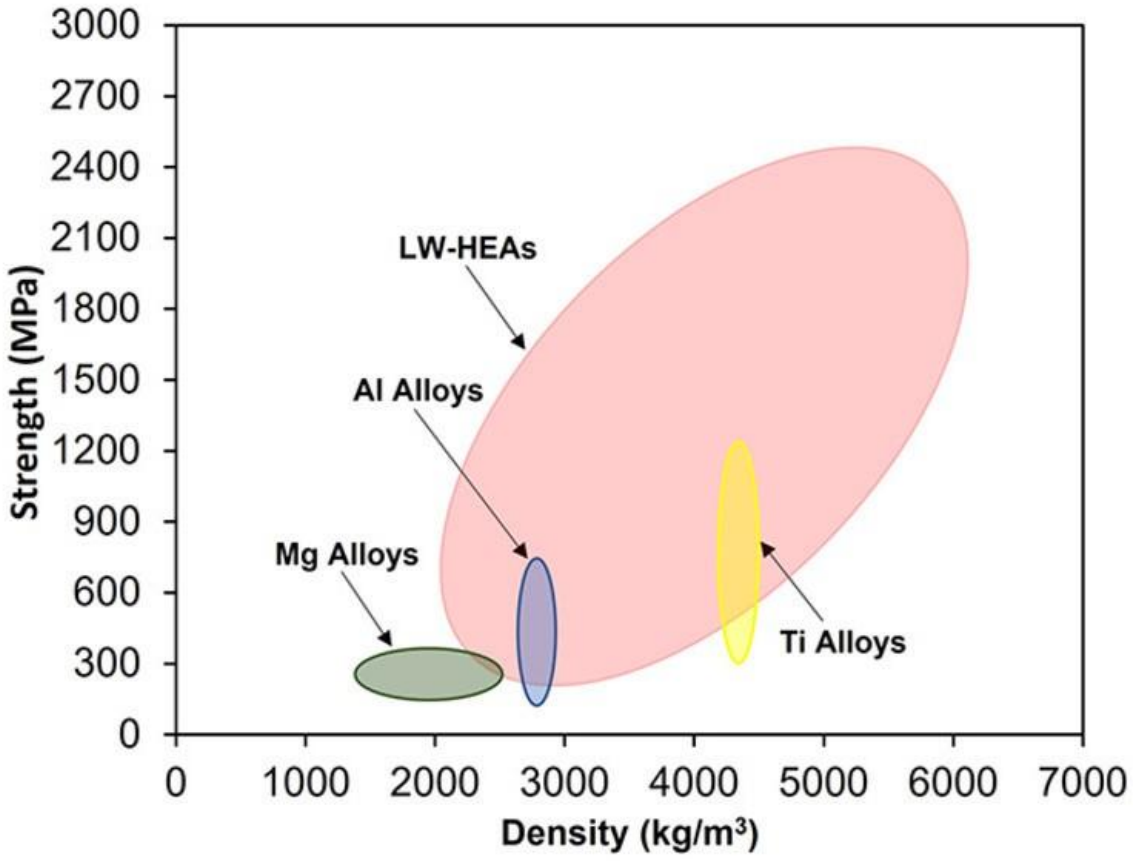


**Figure 2-1** Strength vs. density diagram for HEAs and conventional alloys [26].

From the thermodynamics aspect, high-entropy effect favours alloys of as-cast state with high configuration entropy to form solid solution structure in HEAs, which are relatively more stable than intermetallic structure or amorphous structures [28, 29]. Therefore, this intrinsic property of high configuration entropy leads it to enhanced chemical and mechanical stability than traditional alloys [14, 30].

From the aspect of kinetics, the sluggish diffusion effect plays a crucial role in the thermal and mechanical stability of HEAs [31-33].The presence of multiple principal elements, each with different atomic sizes, inhibits the formation of direct diffusion pathways. This complexity

raises the activation energy required for diffusion, thereby slowing the diffusion rate [33, 34]. The reduced diffusion rate significantly contributes to the overall stability of HEAs under thermal and chemical stresses.

From the aspect of structure, lattice distortion makes efforts on strengthening the mechanical properties of HEAs [35-38]. In HEAs, atoms of varying sizes, lattice potentials and chemical bond configurations occupy the same lattice matrix randomly, leading to significant lattice distortion [38]. This distortion enhances the mechanical strength and thermal stability of HEAs, further differentiating HEAs from traditional alloy designs.

Conclusively, by utilising the three mechanisms above, HEA performs as a capable candidate of bond coat alloys satisfying the demands of oxidation resistance and durability.

### 2.1.3 MCrAlY alloys

MCrAlY alloy, one of the most practical HEAs, has been widely utilised as a durable anti-corrosion bond coat material satisfying demands of high turbine engine efficiency due to its excellent stability. MCrAlY belongs to the system of transition metal HEAs (TM-HEAs), which are mainly composed by transition metal elements (Co, Cr, Ni, etc) and typically contain 6–12 wt% Al and 17–30 wt% Cr [39]. TM-HEAs have intrinsic properties of low density, high corrosion resistance, outstanding thermal stabilities and mechanical strength at high temperature and extrinsic property of acceptable cost, which is a competent candidate as a protective bond coat material for turbines [40, 41].

MCrAlY alloy has two primary phases, intermetallic bcc-β (NiAl or CoAl) phase and solid solution fcc-γ (NiCo or NiCr) phase [3]. The ability of anti-corrosion of MCrAlY is mainly

obtained by the extracted Al and Cr from β phase and γ phase forming an intact and dense aluminium oxide layer and chromium oxide layer to prevent intrusion and further corrosion by oxygen and nitrogen [40-44], which can be found in **Figure 2-2**. Co served as a role of mechanical strength provider in MCrAlY alloy [45]. Y is responsible for oxide scale adhesion at severe temperature [46].

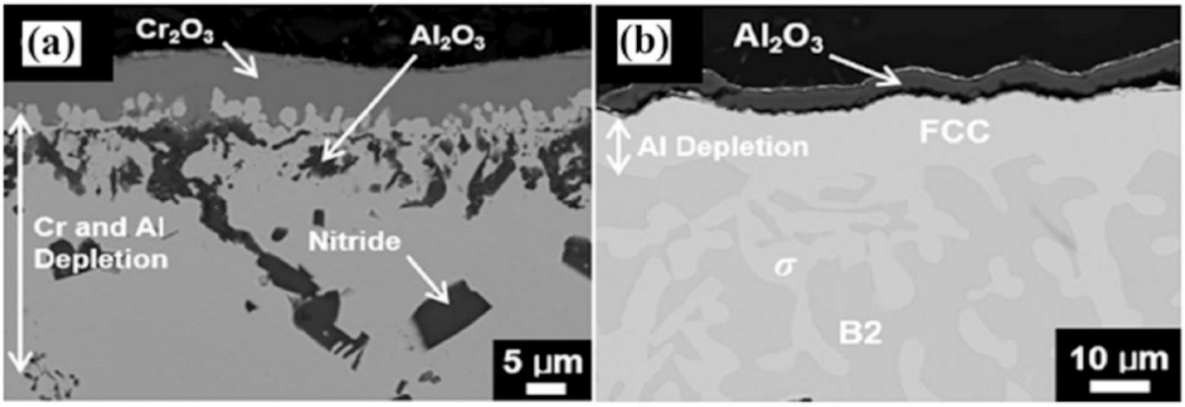


**Figure 2-2** Cross-sectional view of oxide scales on the MCrAlY alloys of (a) high Cr content and (b) high Al content [40].

Though the microstructure and oxidation characteristics of MCrAlY have been widely reported, it is mostly limited to the commercially available compositions. These commercial MCrAlY materials are facing great challenges in meeting further extreme conditions due to the degradation caused by inter-diffusion between the coating and substrates[47, 48], which requires better oxidation resistance due to accelerated oxidation rate at high temperature. Thus, designing and developing novel MCrAlY compositions and microstructures are necessary to solve these challenges.

### 2.1.4 Effects of Cr-to-Al ratio

In alloys containing Cr and Al, the Cr-to-Al ratio significantly influences microstructure, mechanical strength, and oxidation resistance. When the Cr and Al content change, it is the competing growth of spinel oxides, $Cr_2O_3$ and $Al_2O_3$ that governs the oxidation kinetics of MCrAlYs [49]. Content of aluminium offers excellent oxidation resistance and content of chromium offers excellent mechanical strength. However, the oxidation resistance of chromium is not as good as aluminium, because $Cr_2O_3$ is not as dense as $\alpha$-$Al_2O_3$, allowing reactive gases to diffuse more easily, and failures in sealing the surface and the potential evaporation of chromium oxide can accelerate coating degradation [50].

There are studies discovered some rationales of the Cr-to-Al ratio. Chen et al. [51] reported that in pure Cr-Al alloys, high Cr-to-Al ratio can leads to the formation of loosely structured oxide protective layers, while low Cr-to-Al ratio can degrade the mechanical strength of the alloys. Liu et al. [52] suggested a limited Cr-to-Al ratio because high aluminium content can create porous features that minimally impede the inward diffusion of oxygen if nitride is present. More recently, to reveal the effects of Cr-to-Al ratios on the oxide growth, Zeng et al. [53] investigated the oxidation behaviour of CrAl coatings by carefully controlling the atomic ratios of Cr-to-Al and found the transition of $Al_2O_3$ to $Cr_2O_3$ at appropriate Cr-to-Al ratios. Additionally, Pohler et al. [54] noted that for alloys at low Cr-to-Al ratio, a secondary layer of low crystallinity may form beneath the outer layer.

Chromium and aluminium, due to their similar medium metal activities, can oxidise simultaneously to form protective $\alpha$-$Al_2O_3$ and $Cr_2O_3$ scales at high temperatures, as a pair of competing oxides according to their activation energy. While aluminium is more reactive and

forms a dense alumina layer that effectively prevents further oxidation, chromium can also be oxidised significantly, with its oxide forming on the alumina layer due to a higher outward diffusion rate.

Aluminium contributes to oxidation resistance by creating a compact alumina layer, whereas chromium forms a competing oxide, chromium oxide. The microstructure of the oxides formed can be influenced by several factors, including the atomic ratio of Cr and Al, temperature, and heating duration. To maintain the hardness provided by chromium while ensuring effective oxidation resistance from aluminium, it is essential to investigate and interpret the oxidation evolution of CoNiCrAl alloys at varying Cr-to-Al ratios.

## 2.2 Vacuum arc melting

### 2.2.1 Background and methods

To meet the stringent demands for high purity, low defect rates, and robust mechanical strength in casting HEAs, vacuum arc melting (VAM), an advanced alloy casting technique is utilised to cast high quality metal ingots [55]. The advantages of VAM are achieved by its unique casting environment. The method utilises direct current to melt raw materials into alloy ingots within a vacuum furnace (see **Figure 2-3**). This vacuum setting prevents the molten metal from contacting with any reactive gases, thereby ensuring the purity of the final product. Additionally, the thorough melting and mixing processes stabilise the product, minimizing defects and inhomogeneities that could complicate subsequent analyses. Furthermore, the utilisation of electricity allows VAM to adjust electrical input accurately and timely to control temperature, enabling the precise execution of complex casting procedures.

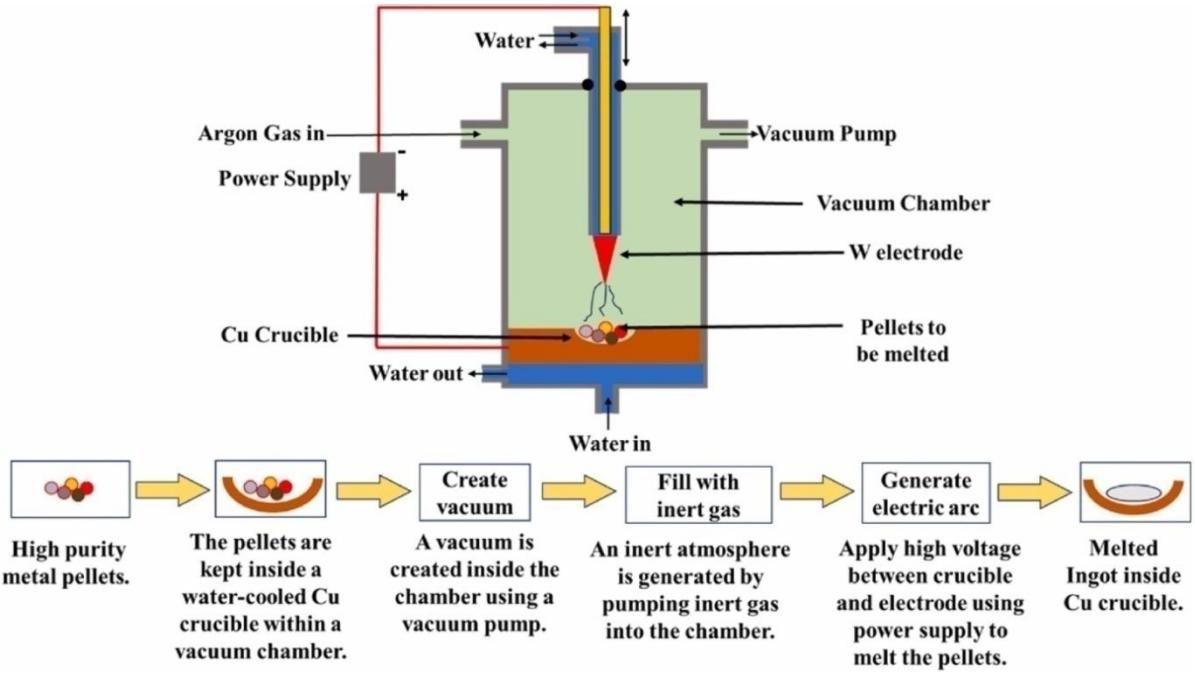


**Figure 2-3** Schematic diagram and procedures of VAM [55].

VAM not only enhances the purity and reduces defects in the produced alloys, but also it improves their mechanical strength. The rapid solidification process can be achieved by VAM to produce columnar dendritic structure and interdendritic segregation, which can confer additional strength to HEAs [56].

Though the method of VAM has several advantages compared to traditional casting methods, the rapid solidification step associated with VAM can lead to the formation of amorphous structures, which may replace solid solution structures [57, 58]. The presence of amorphous phases can negatively impact the mechanical strength and thermal stability of HEAs, which is unfavoured in alloy casting. Therefore, additional processing steps are often required to transform amorphous alloys into solid solution structures for products of VAM.

### 2.2.2 Application and performance

VAM is particularly advantageous for the development of HEAs, as its highly controllable parameters align satisfying the design requirements of these materials. First of all, the ability to precisely control temperature during the casting process allows for the tailored design of grain size and uniformity in HEAs. Empirical evidence suggests that VAM can enhance ductility, strength, and other desired mechanical properties, as well as improve chemical and thermal stability [59-61]. Moreover, VAM facilitates the casting of alloys with mixed microstructures. HEAs characterised by multi-phase structures have shown a potential of improving high temperature performance compared to their single-phase counterparts [62]. This multi-phase structure is a result of the rapid solidification process employed in VAM.

For instance of performance, Cieslak et al. [63] demonstrated that CrAlFeCoNi alloys produced using the VAM method exhibit superior corrosion resistance compared to those casting via sintering techniques. Similarly, Wang et al. [60] reported that AlCrFeCoNi HEAs fabricated by VAM show enhanced overall mechanical strength compared to alloys produced using traditional methods. Zhang et al. [61] proposed the same improvement in mechanical properties in CoCrFeNiCuAl alloys casted using the VAM technique.

## 2.3 Heat treatment

A heat treatment is necessary to homogenise phase distribution in HEAs for their complex microstructures. Heat treatment is a process that involves controlling temperature through specific procedures to alter the microstructure of metals. Commonly, this method can make significant changes to the mechanical properties of alloys, and their hot corrosion resistance

also can be varied.

For instance, as illustrated in **Figure 2-4**, the grain size of oxidised bond coats subjected to heat treatment is larger than that of untreated bond coats. This observation suggests that the oxide scale formed during heat treatment is more intact, which in turn reduces the diffusion path for oxygen. Consequently, the oxidation resistance of CoNiCrAlY alloys that have undergone heat treatment is significantly stronger compared to those that have not, highlighting the critical role of heat treatment in influencing oxidation behaviour.

Moreover, alloys in the as-cast state may contain amorphous phases if they are undercooled during the casting process [37]. A proper heat treatment with a low cooling rate can facilitate a phase transformation from an amorphous structure to solid solution or intermetallic compounds.

Furthermore, several parameters of heat treatment, including temperature, duration, and ambient pressure, can significantly affect the microstructure and oxidation resistance of CoNiCrAlY alloys. For instance, Keller et al. [64] demonstrate that a low-pressure environment during heat treatment can promote the migration of the bcc-β phase to the surface, as depicted in **Figure 2-5**. Similarly, Jung et al. [65] report that lamellar patterns of the γ phase can form in AlTi alloys through heat treatment, attributing these patterns to enhanced thermal stability [66]. Meng et al. also noted that an optimal heat treatment can enhance adhesion strength [67].

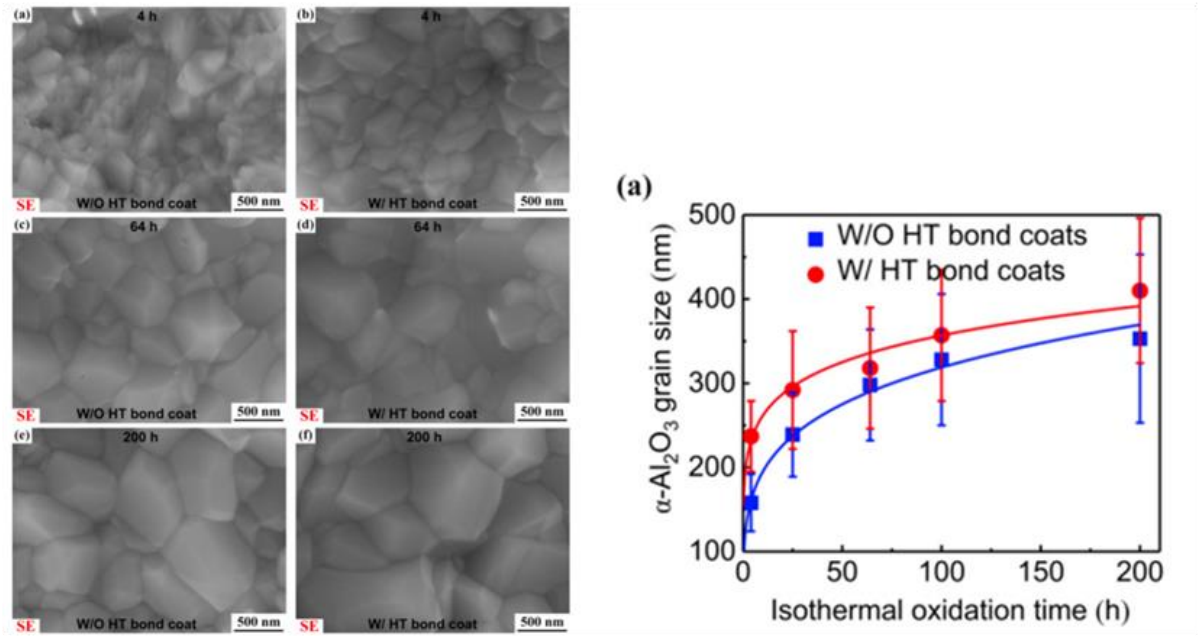


**Figure 2-4** Oxidation rates of CoNiCrAlY alloys with heat treatment vs. oxidation rates of CoNiCrAlY alloys without heat treatment [68].

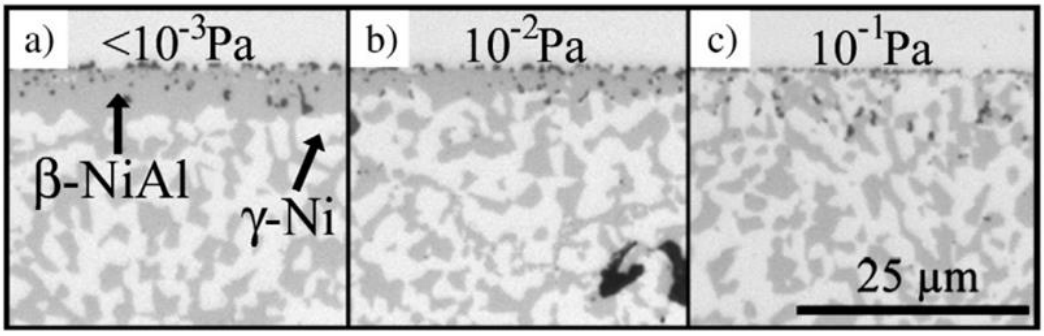


**Figure 2-5** Microstructure of CoNiCrAlY alloys at different heat treatment pressure [64].

For MCrAlY alloys, the fundamental purpose of proper heat treatment is to distribute the bcc-β phase more homogeneously within the fcc-γ phase matrix [68]. This transformation can significantly enhance the chemical homogeneity and thermal stability of MCrAlY alloys.

These studies underscore the importance of heat treatment conditions in modifying the microstructure of MCrAlY alloys and enhancing their oxidation resistance.

### 2.4 Gap in the literature

Previous studies mainly focus on the oxide growth mechanism using the commercial MCrAlY powder compositions [14]. It has been widely recognised that a dense alumina scale can form at the material surface, but a dual layer of oxides consisting of an outer layer of spinel oxides and an inner layer of alumina is also found, depending on the heat treatment history [17]. It has been reported that Cr can facilitate the growth of stable $Cr_2O_3$ and increase the service time of the CoNiCrAlY materials. However, none of the previous studies have comprehensively investigated the competing oxide growth mechanism at different Cr-to-Al ratios. Since Cr content can change the oxide growth method of CoNiCrAl alloy, the competing growth mechanism of $Cr_2O_3$ and $Al_2O_3$ at different Cr-to-Al ratios is valuable to be studied. More importantly, the exploration in the oxidation mechanism will be able to develop novel CoNiCrAlY-based high entropy alloys with improved thermal stability and oxidation resistance. Though there is a paper reported the effects of Al content on the microstructure and oxidation behaviour of CoNiCrAlY alloys, it is limited to high Al content alloys [69]. The growth of competing oxides, such as $Cr_2O_3$ is only applicable in oxidation of low Al content alloys because Al is relatively active thus Al would be prior to be oxidised unless Al is not insufficient. The microstructure and oxidation behaviour of low Al content alloys is still needed to be investigated since the impacts of Cr content were ignored by the studies focusing on Al content. To develop novel composition and microstructure of the CoNiCrAlY alloys, the heat treatment temperature and time to obtain a homogeneous phase distribution with improved oxidation resistance also need to be studied for improvement.

# Chapter 3 Methodology

### 3.1 As-cast sample preparation

Five as-cast CoNiCrAl alloys of different Cr-to-Al ratios were prepared using the vacuum arc melting process. The nominal compositions of these alloys at different Cr-to-Al atomic ratios are detailed in Table 1, which cover the composition of β phase dominating, which allow exclusive alumina growth (ratio 0.3), the reference composition of commercial MCrAlY powder (Amdry 9951, Praxair CO-210-24) with ratio 1.3, and the composition of γ phase dominating, which allow intact chromium oxide layer grows (ratio 2.8) [53, 70-73]. The compositional ranges of Al and Cr in the samples were extended beyond those of conventional MCrAlY alloys to investigate the fundamental oxidation mechanisms under extreme conditions. The Cr-to-Al ratios of samples were controlled by the weight of Cr and Al added while Co and Ni were kept constant. Yttrium, typically only included at 0.5 wt% in commercial MCrAlY powders, is commonly added to improve oxide adhesion and reduce the exfoliation of oxide scales [74, 75], but the risk of oxide scale exfoliation is minimal in laboratory. Therefore, it was excluded from the alloy composition due to its limited proportion and negligible effect on the phase equilibria [19].

The vacuum arc melting was conducted in pure argon (99.99%) at a pressure of 700 mbar using a non-consumable vacuum arc melting furnace (EbmundBüehler AM200) to manufacture the as-cast samples. High purity(>99.99%) Co, Ni, Cr, and Al ingots (provided by Yijinxincai Co.) were placed in an alumina crucible within the furnace. To prevent oxidation during the casting process, oxygen in the chamber was removed by evacuating the furnace to a pressure of $9 \times 10^{-4}$ bars and then backfilled with pure argon gas three times to create an oxygen-free

environment. The raw metal ingots were melted at temperatures ranging from 4700 to 5700 °C using an electric arc maintained at 250-500 A. To ensure thorough mixing, the molten metal was stirred at a current of 5 A for 5 minutes and repeated for six times. The crucible was inverted after each vacuum arc melting cycle to promote chemical homogeneity of the samples. The molten metal was then casted into a mould with 250 mm radius and 14.9 mm depth, and after complete cooling and solidification, the as-cast alloys were cut into cuboids of 10 mm × 10 mm × 5 mm using wire electro-discharge machining (WEDM, Mitsubishi MV2400S) for further treatments and inspections.

**Table 3-1** Nominal composition of the as-cast CoNiCrAl alloys.

| Sample# | Cr:Al (atomic ratio) | Co (wt %) | Ni (wt %) | Cr (wt %) | Al (wt %) |
|---|---|---|---|---|---|
| 1 | 0.3 | 39.4 | 31.7 | 10.6 | 18.3 |
| 2 | 0.8 | 39.4 | 31.7 | 17.5 | 11.4 |
| 3 | 1.3 | 39.4 | 31.7 | 20.8 | 8.1 |
| 4 | 1.8 | 39.4 | 31.7 | 22.4 | 6.5 |
| 5 | 2.8 | 39.4 | 31.7 | 24.4 | 4.5 |

### 3.2 Heat treatment

According to previously published work in a wide range of heat treatment attempts [19], a homogenisation heat treatment is necessary to obtain even phase distribution in the as-cast alloys. The heat treatment was performed to the as-cast CoNiCrAl alloys at 1300 °C for 25 hours in an argon atmosphere to prevent the formation of impurities from reactive gases. Prior to treatment, the surface of the alloys was polished to ensure purity and smoothness. The alloys

were placed in separate alumina crucibles within a vacuum furnace. The chamber was evacuated to a pressure of $9\times10^{-4}$ bars and then backfilled with pure argon (>99.99%) three times to remove any residual oxygen. After heating the as-cast alloys at 1300 °C for 25 hours, a natural cooling was employed. This cooling process took approximately 10 hours to bring the alloys down gradually to the room temperature.

### 3.3 High temperature oxidation

An isothermal high temperature oxidation was conducted on the alloys after heat treatment. The alloys were carried in separate alumina crucibles and subjected to oxidation at 1100 °C in an air furnace. Each set of the alloys of different Cr-to-Al ratios were then oxidised at intervals of 2 h, 10 h, 25 h, 50 h, and 100 h. A 400-minute preheat was employed prior the high temperature oxidation, followed by a 600-minute natural cooling stage.

### 3.4 Microstructure characterisation

The phases present in the alloys were identified by Bruker AXS D8 Advance XRD, with a scanning step of 4 s for every 0.02°, and a scanning range of 2θ from 20° to 100°. The output from XRD was processed using MDI Jade 9 to identify the characteristic peaks of different phases. The surface morphology of the oxidised alloys and cross-sectional microstructures at various oxidation stages at boundaries were inspected by ZEISS Gemini1 FE-SEM at 15 kV extra high tension (EHT) after a mirror-like surface finish was obtained by successively grounding and polishing. The alloys were gold-sprayed prior to surface morphology inspection. Elemental compositions of phases before and after heat treatment were qualitatively analysed

by EDS. Results were averaged from three trials to ensure representativeness. Elemental distribution and concentration of Co, Ni, Cr, Al, O, and N were assessed via EDS mapping, conducted simultaneously with SEM imaging to correlate compositional data with the phases previously identified by XRD. The volume fractions of each phase were further analysed in image processing software, ImageJ. The images were initially processed with noise despeckling, followed by conversion from RGB to 8-bit format. The Image-Adjust-Threshold function was then applied to determine the volume fraction of the phases. The threshold's LUT value was set at the minimum between two peaks, allowing for distinct identification of the two phases. The volume fraction of the γ phase (the brighter phase) was then displayed.

### 3.5 Strengths and limitations

This study employs a comprehensive set of inspection methods, including SEM, EDS, and XRD, with cross-validation. The compositions, identified phases, and microstructures were compared with those reported in relevant studies. Additionally, the experimental threshold for chromium oxide formation was compared to the theoretical value. However, the study has some limitations, such as the potential risk of yttrium removal and the limited sample size, which may lead to errors.

# Chapter 4 Results and discussion

### 4.1 Microstructure of the as-cast CoNiCrAl alloys

**Figure 4-1** shows the microstructure of the initial stage of the samples, as-cast CoNiCrAl alloys. The alloys at ratio of 0.8 to 1.8 (**Figure 4-1**(a-d)) have a typical lamellar eutectic structure with a dark β-(NiAl) phase and a bright γ phase. Unclear boundaries between β and γ phase were noticed in as-cast CoNiCrAl alloy at ratio of 0.3 in **Figure 4-1**(a) due to the excess amount of scattered γ phases precipitation without aggregation by rapid solidification in casting process[19]. In contrast, in **Figure 4-1**(e), the as-cast alloy at Cr-to-Al ratio of 2.8, has a uniform γ phase with trace AlN detected, and no β phase was observed. The area fraction of impurities in **Figure 4-1**(e), mostly AlN, is about 2% in cross-section on the surface. Phase of oxide was not found in the as-cast alloys. The identity of phases and their proportions were further confirmed by the result of EDS and XRD analysis in **Section 4.2** and **Section 4.3**.

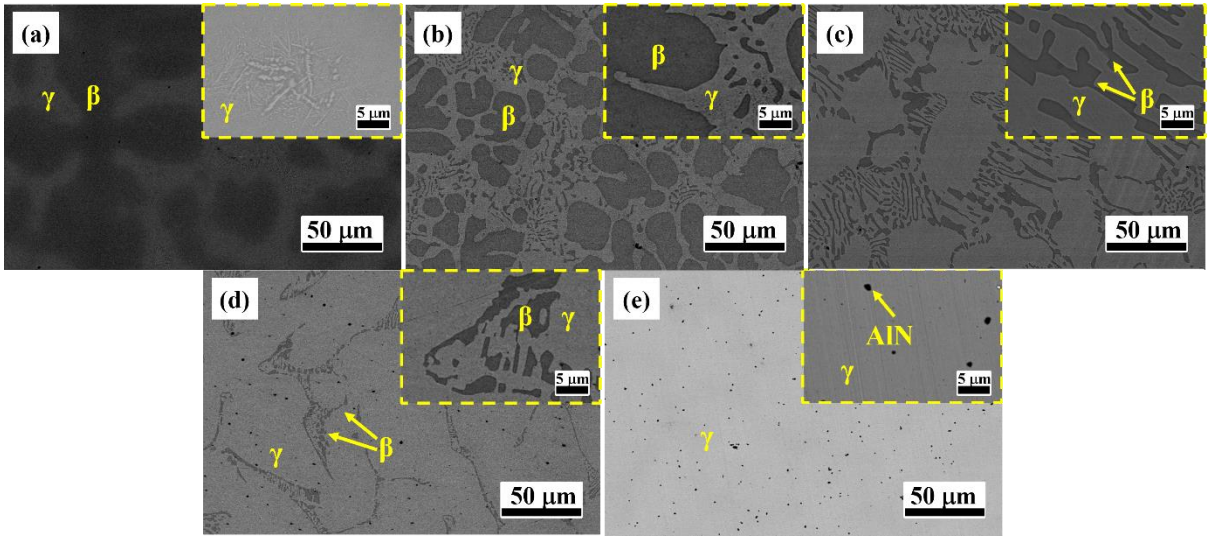


**Figure 4-1** Microstructure of the as-cast CoNiCrAl alloys at Cr-to-Al ratio of: (a) 0.3; (b) 0.8; (c) 1.3; (d) 1.8; (e) 2.8 before heat treatment.

To homogenise the as-cast CoNiCrAl alloys, 25 hours 1300°C heat treatment in closed furnace was applied, and the microstructure of CoNiCrAl alloys after heat treatment can be seen in **Figure 4-2**. Heat treatment improved the structural homogeneity and stimulated the major phase to grow continuously and the minor phase to accumulate, and the balance of β and γ phase was achieved at ratio 0.8 (see **Figure 4-2**(b)), where distributions of two phases are nearly equivalent, thus both phases appear to be continuous and large patterns. Nucleation of minor phases was achieved, which can be conducted by comparing **Figure 4-1** and **Figure 4-2**. Any lamellar patterns of phases in the alloys were eliminated by the heat treatment. Additionally, the boundaries between β and γ phase were clarified. The most significant change was gained by the alloy at ratio of 0.3 in **Figure 4-2**(a). It gained clear boundaries between β and γ phase and clear γ phase could be recognised after phase redistribution achieved by heat treatment.

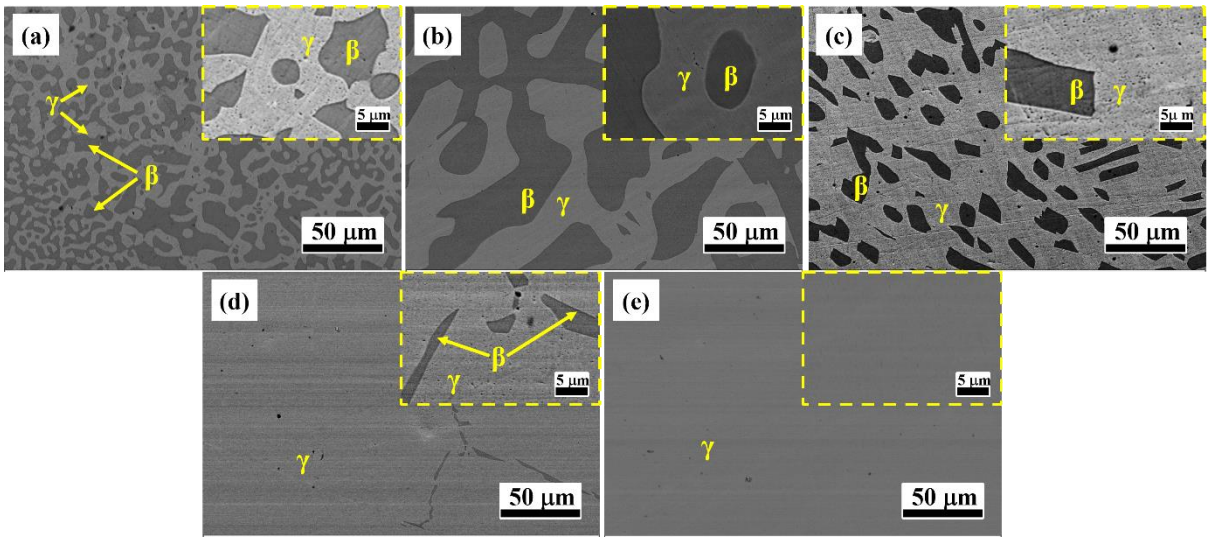


**Figure 4-2** Microstructure of the as-cast CoNiCrAl alloys at Cr-to-Al ratio of: (a) 0.3; (b) 0.8; (c) 1.3; (d) 1.8; (e) 2.8 after heat treatment.

### 4.2 Phase proportions and compositions

**Figure 4-3** is a diagram of β and γ phase fractions illustrating the phase changes of the as-cast CoNiCrAl alloys by heat treatment. The proportion of β phase in the alloy at ratio of 0.3 was dropped slightly, which replaced by the proportion of γ phase. For the alloy at ratio of 0.8, which huge β and γ phase patterns were generated, **Figure 4-3** indicates the proportions of β and γ phase are approximately 50%, which not only allow nucleation of "minor phase" but also of the "major phase". As a result, the process of nucleation was prolonged and enlarged. β and γ phase nucleate simultaneously and equivalently to form larger phase patterns. In the alloys at ratio of 1.3-2.8, β phase becomes the minor phase and is nucleated to shorter patterns instead of lamellar structures. The decrease in proportion of β phase with increase in Cr-to-Al ratios can be explained that the overall Al content in the alloy decreases with Cr-to-Al ratio increases. Since the proportion of the β phase is closely associated with the Al content, a decrease in the β-phase proportion is expected at high Cr-to-Al ratios, as indeed seen in **Figure 4-3**. In the alloys at Cr-to-Al ratio of 1.8, uniform γ phase with trace AlN, and small proportion of β phase can be identified. The volume fraction of γ phase is proportional to Cr-to-Al ratio as expected, proven by software ImageJ quantification, and exclusive γ phase was observed in the alloys at ratio of 2.8 as shown in **Figure 4-3**.

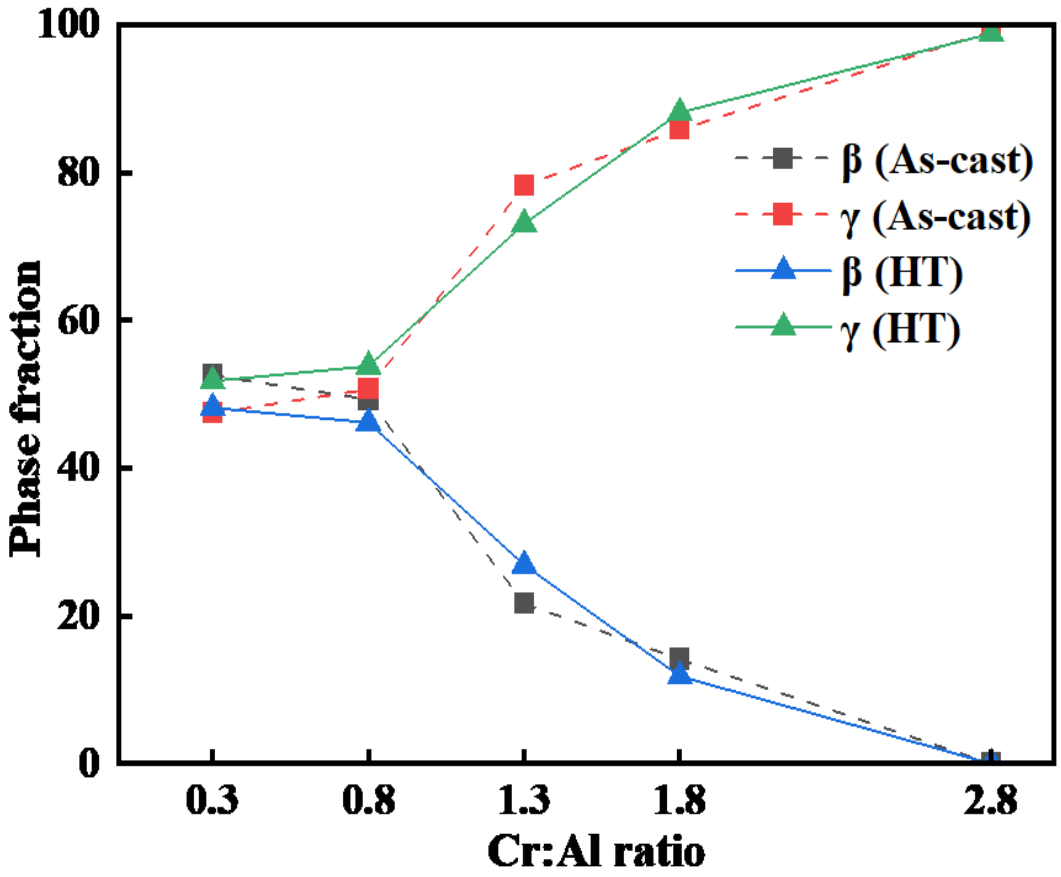


**Figure 4-3** β and γ phase fractions of the as-cast and HT CoNiCrAl alloys at various Cr-to-Al ratios.

**Figure 4-4** displays the elemental composition changes of β and γ phase by heat treatment. The changes of phases are not influential, but roughly follow a trend. It can be induced that Ni and Al transferred from γ phase to β phase, contrarily, Co and Cr transferred from β phase to γ phase in exchange. The alloys at ratio of 2.8, which is a single γ phase, exhibit an unexpected composition change, and the compositions of the alloys after heat treatment are more coherent to the nominal composition designed, which proves the homogenisation effect of the heat treatment.

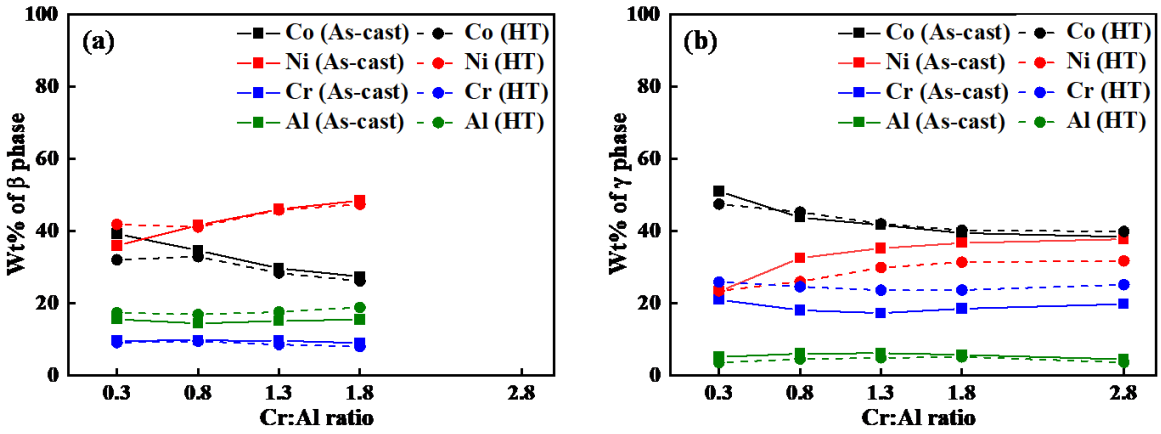


**Figure 4-4** Composition evolution of (a) β phases and (b) γ phases in the as-cast and HT CoNiCrAl alloys at various Cr-to-Al ratios.

### 4.3 Phase identification

XRD patterns of CoNiCrAl alloy at various stages of oxidation at 1100°C are shown in **Figure 4-5**. Characteristic peaks of fcc-γ phase, spinels and $Al_2O_3$ are noticed in all alloys. $Cr_2O_3$ is found in the alloy at ratios of 1.8 and 2.8 (see **Figure 4-5**(d)-(e)), and bcc-β phase is found in the alloy at ratio of 0.3-1.8 (see **Figure 4-5**(a)-(d)). The result of XRD is substantially coherent to that of EDS, beside AlN. Though the existence of AlN is proved by EDS in oxidised samples, the characteristic peaks of AlN are unable to be found in the output of XRD. This contradiction should be caused by two factors. On one hand, the proportion of AlN is small, so the signal of AlN can be weak enough to be covered by the background noise. On the other hand, the depth limitation of XRD detection prevents it from effectively detecting AlN, as the oxide layer hinders access to the material.

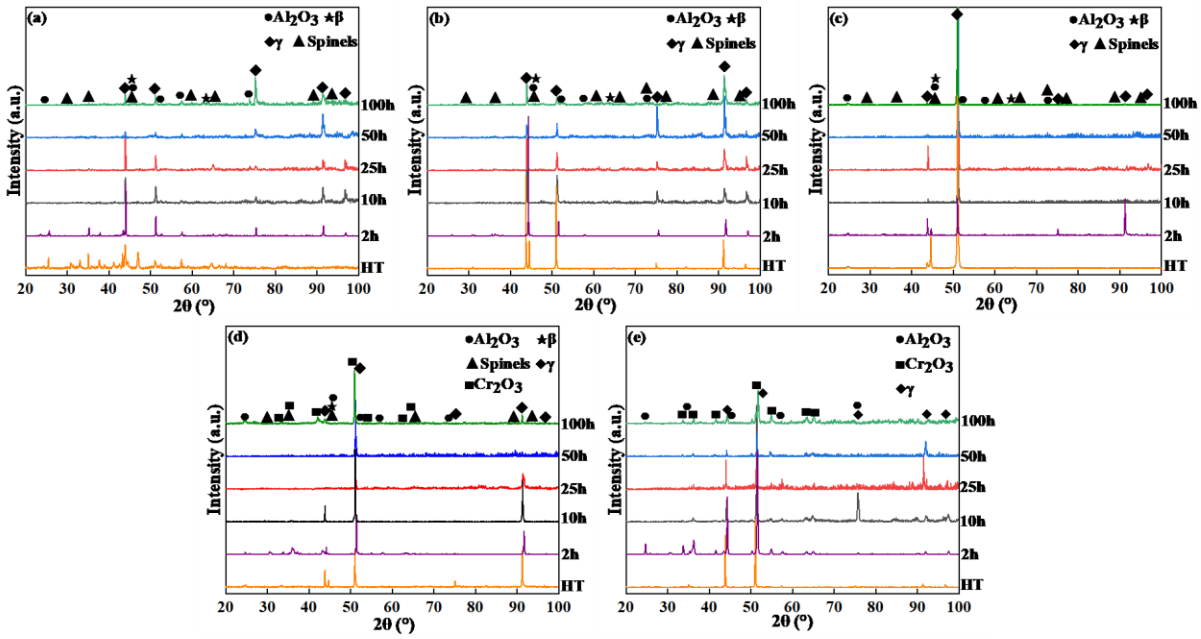


**Figure 4-5** XRD patterns of HT CoNiCrAl alloys at Cr-to-Al ratios of: (a) 0.3, (b) 0.8, (c) 1.3, (d) 1.8 and (e) 2.8 after 2 h, 10 h, 25 h, 50 h, and 100 h oxidation.

**Figure 4-5** shows changes between the patterns of the early and later stages of oxidation. At early oxidation stage of low Cr-to-Al ratio samples (see curves between HT and 10 h in **Figure 4-5**), formation of $Al_2O_3$ extracts Al content from β phase, which forms extra γ phase layer beneath the oxide layer. Hence the signal of γ phase is amplified and the signal of β phase is reduced. At later oxidation stage of low Cr-to-Al ratio samples (see curves between 100 h and 25 h in **Figure 4-5**), formation of continuous alumina layer on top amplifies the signal of $Al_2O_3$ after long time oxidation and shades the signal of γ phase.

In high Cr-to-Al samples (see **Figure 4-5**(d)-(e)), simultaneous formation of $Al_2O_3$ and $Cr_2O_3$ does not change the dominating status of γ phase or create any new β phase. The signals of $Al_2O_3$ and $Cr_2O_3$ both relatively amplified in the later oxidation stage, which indict a steady growth of both oxides.

The signal of spinels is not significant. The formation of spinels is low on surface after oxidation.

### 4.4 The microstructure of the oxidised CoNiCrAl alloys

The surface morphology of oxide scales on CoNiCrAl alloys at 1100 °C for various oxidation stages is shown in **Figure 4-6.** By EDS elemental identification (average compositions of typical oxides by EDS can be referred in **Table 4-1**), both oxides, $Al_2O_3$ and $Cr_2O_3$ were identified as dark smooth but discontinuous scale growing on top of the substrate, and spinel oxide (in the form of $(Ni,Co)(Al,Cr)_2O_4$) is identified by its porous structures. In low Cr-to-Al ratio samples (see **Figure 4-6**(a-i)), layer of alumina can be observed just after 2 h oxidation, and the surface area of $Al_2O_3$ is proportional to the concentration of Al and the oxidation time. On contrary, in high Cr-to-Al ratio alloys (see **Figure 4-6**(m-o)), only growth of $Cr_2O_3$ is observed on the surface. Though it is still possible that there can be some $Al_2O_3$ on the surface, $Cr_2O_3$ is definitely dominating. The surface morphology at ratio of 1.8, the alloys reveals a unique oxidation process, which is a Cr-to-Al ratio threshold of $Cr_2O_3$ formation. On its surface, $Al_2O_3$ is found after 2 h oxidation but replaced by $Cr_2O_3$ after 10 h and 100 h oxidation. $Al_2O_3$ is still possible to exist on surface because it was found in cross-sectional view of CoNiCrAl alloy after 10 h oxidation in **Figure 4-8**(d) but it can be covered by spinels or its proportion is too low to be sampled in surface morphology inspection.

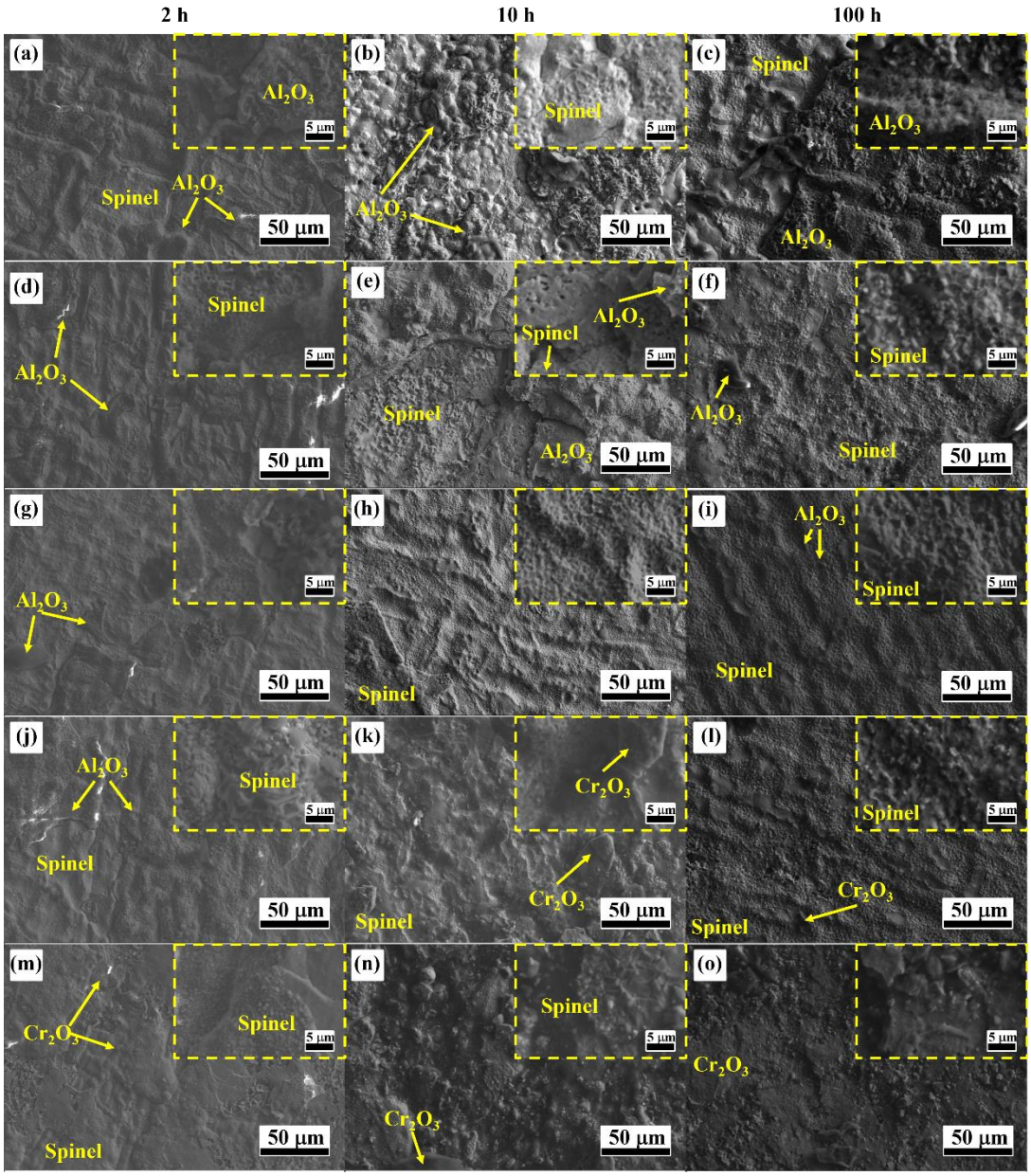


**Figure 4-6** Surface morphologies of the CoNiCrAl alloys at Cr-to-Al ratios of: (a-c) 0.3, (d-f) 0.8, (g-i) 1.3, (j-l) 1.8, and (m-o) 2.8 after oxidation at 1100°C.

**Table 4-1** Typical compositions of oxides in CoNiCrAl alloys by EDS analysis

| Element | Spinel (at %) | $Al_2O_3$ (at %) | $Cr_2O_3$ (at %) |
|---|---|---|---|
| Al | 4.4 | 35.4 | 0 |
| Cr | 15.2 | 7.4 | 31.5 |
| Co | 19.7 | 0 | 0 |
| Ni | 11.1 | 0 | 0 |
| O | 49.6 | 57.2 | 68.5 |

**Figure 4-7** shows the microstructure of CoNiCrAl alloys after 2 hours oxidation in 1100 °C. From the view of cross-sectioning, it can be indicated that a layer of pure γ phase was formed underneath the aluminium oxide layer in low Cr-to-Al ratio alloys just after 2 h oxidation. The phenomenon was most obvious in the alloy at ratio of 0.3 (see **Figure 4-7a**). It also can be confirmed by the signal of γ phase by XRD, which was amplified after the oxidation. A dense layer of $Al_2O_3$, with γ phase mixing a few AlN, was observed in alloys except of ratio 2.8. In contrast, in alloys at ratio of 2.8, a dual-layer-structure, with an additional layer of $Cr_2O_3$, was observed on the top of $Al_2O_3$ layer, and the alumina layer is in lamellar pattern instead of in continuous pattern. For the reason that the layer of $Al_2O_3$ kept growing, layer of $Cr_2O_3$ not simply replaces the layer of $Al_2O_3$, but grows on it.

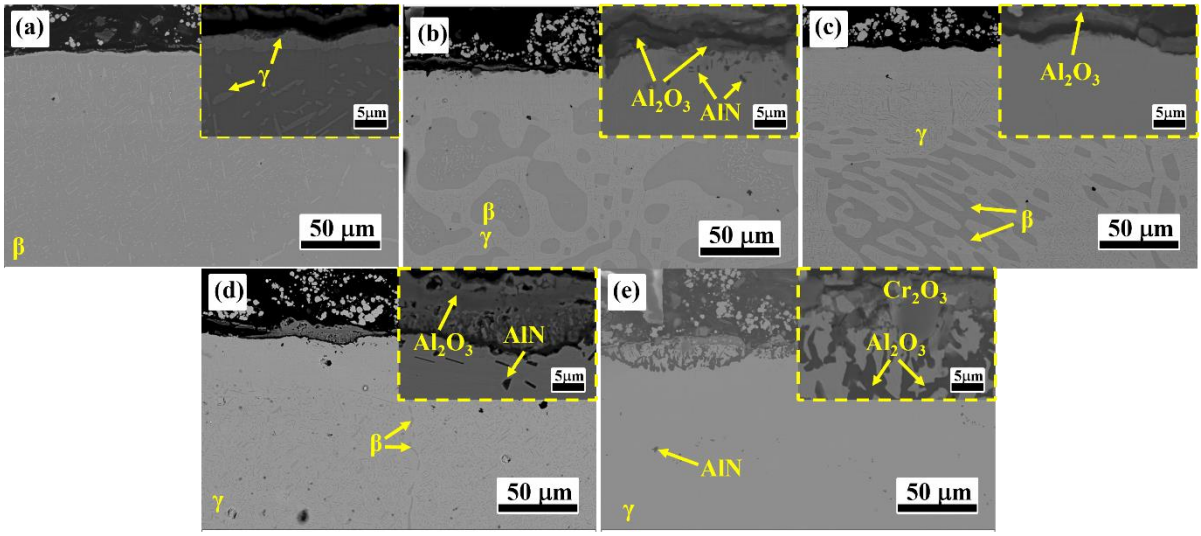


**Figure 4-7** Cross-sectional microstructure of the CoNiCrAl alloys at Cr-to-Al ratios of: (a) 0.3; (b) 0.8; (c) 1.3; (d) 1.8; (e) 2.8 after 2 hours oxidation at 1100 °C.

After 10 h oxidation, both the alumina layer and the γ phase layer (alumina depletion zone) grew thicker, and AlN was observed in deeper positions in alloys at ratio of 0.3-1.3 (see

**Figure 4-8**(a-c)). In the alloy at ratio of 2.8, the layer of $Cr_2O_3$ keeps growing, and both alumina and AlN diffuse deeper and significantly larger (see **Figure 4-8**(d-e)). A critical structure is discovered in the alloy at ratio of 1.8, a mixture of dense $Al_2O_3$ layer and a dual layer structure, with a clear boundary between two structures. It indicates a threshold of exclusive growth of $Al_2O_3$, where two growth mechanisms are well balanced, depending on phase distribution. The co-existence of $Al_2O_3$ and $Cr_2O_3$ layers was confirmed by EDS mapping in **Figure 4-10**, and more AlN was found beneath the dual layer structure than dense $Al_2O_3$ layer.

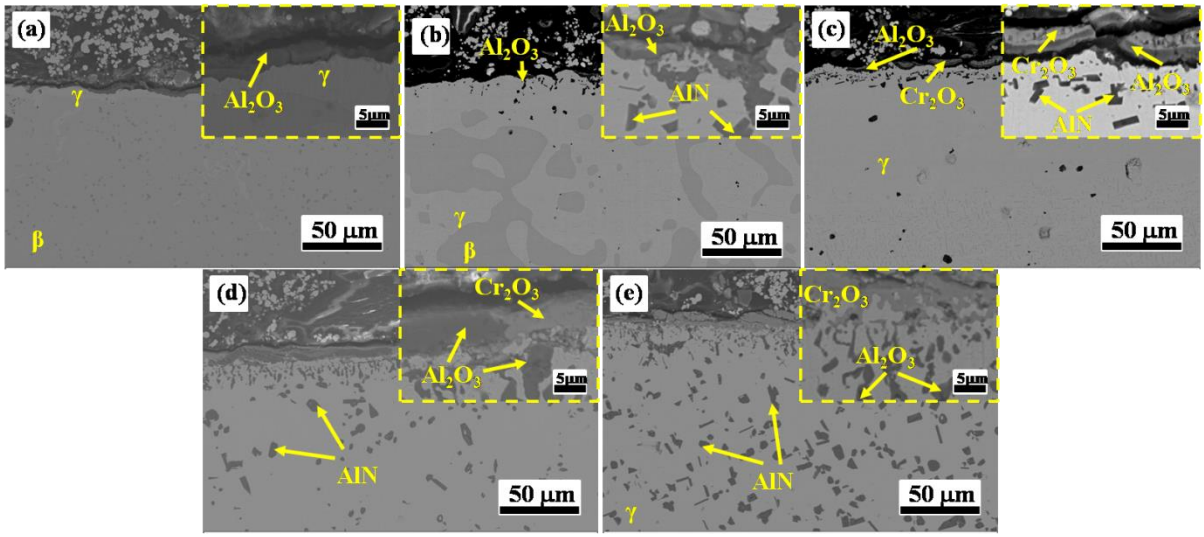


**Figure 4-8** Cross-sectional microstructure of the CoNiCrAl alloys at Cr-to-Al ratios of: (a) 0.3; (b) 0.8; (c) 1.3; (d) 1.8; (e) 2.8 after 10 hours oxidation at 1100 °C.

After 100h oxidation, for the alloys at ratios of 0.3-1.3, dense $Al_2O_3$ layer and AlN was observed. No dense $Al_2O_3$ layer can be observed in alloys at ratio of 1.8 after sufficient oxidation period (see **Figure 4-9**). The structure of alloys at ratio of 2.8 is unchanged but all 3 layers of oxides and nitrite were thickened.

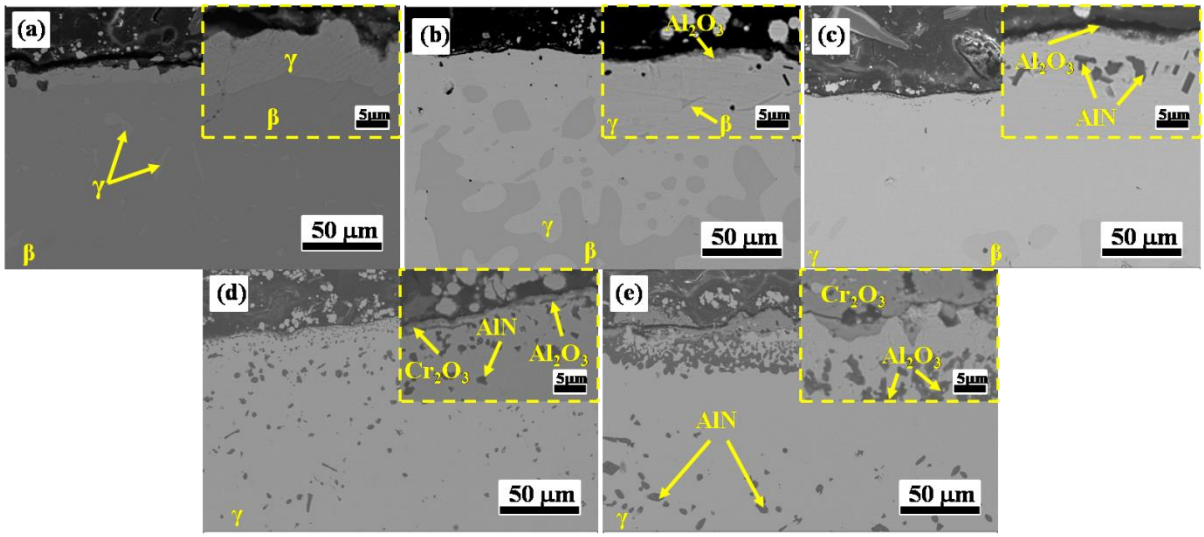


**Figure 4-9** Cross-sectional microstructure of the CoNiCrAl alloys at Cr-to-Al ratios of: (a) 0.3; (b) 0.8; (c) 1.3; (d) 1.8; (e) 2.8 after 100 hours oxidation at 1100 °C.

The distribution of elements after oxidation was visualised by EDS mapping in **Figure 4-10**, which is a sight of view with the most complete microstructure sampled and most phases were included. After 10h oxidation at 1100 °C, surface of the alloy was already essential oxidised. It can be inferred that purities of the oxide layers were high (a few signal of other elements was observed in region of $Al_2O_3$ and $Cr_2O_3$) and intact (no crisscross pattern of phases). In addition, the signal of spinels is still not significant even in cross sectional view, which indicates it is hard to be found not only at the surface of the oxides, but also beneath the top oxide layer.

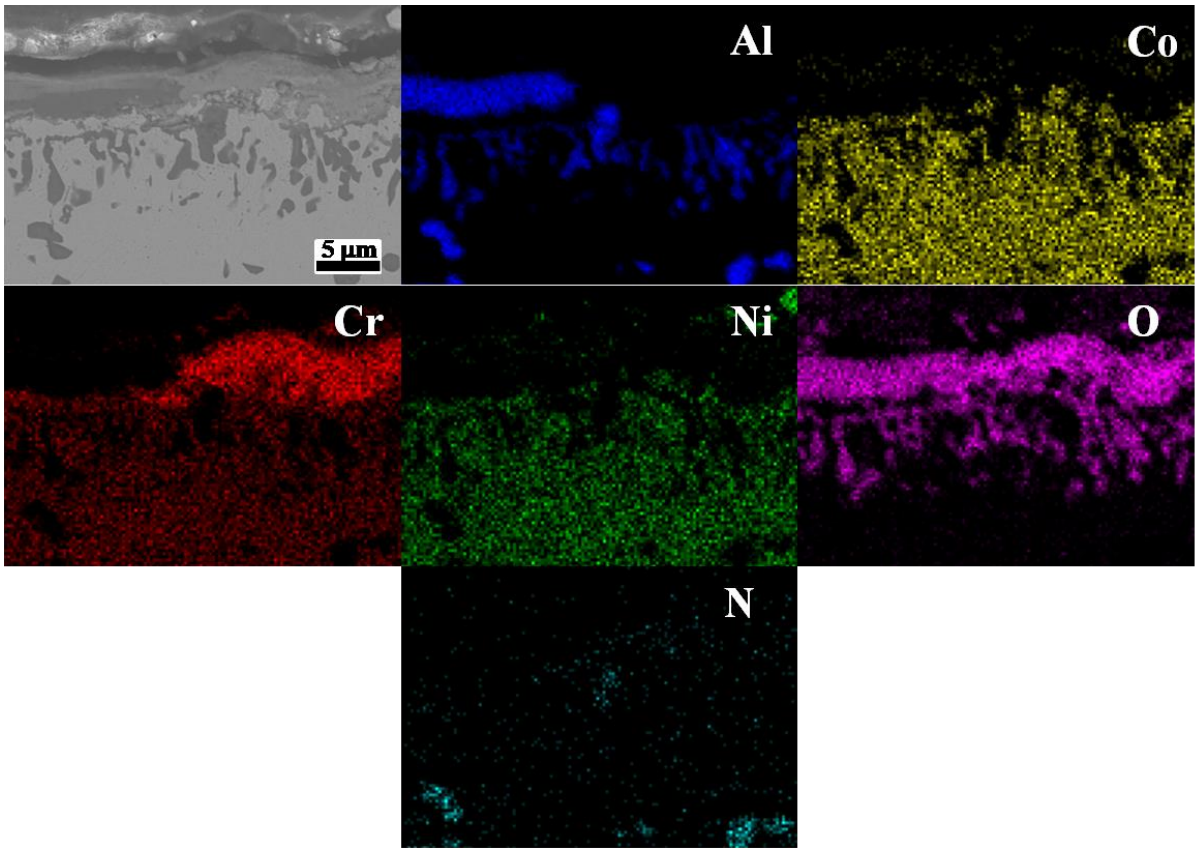


**Figure 4-10** The EDS elemental mapping of oxide and nitride growth in the CoNiCrAl alloys at Cr-to-Al ratio of 1.8 after 10 hours oxidation at 1100 °C.

### 4.5 Growth of competing oxides

The major oxides of the CoNiCrAl alloy formed after oxidation at 1100°C are $Cr_2O_3$ and $Al_2O_3$. The content of other potential oxides, such as NiO and $NiCr_2O_4$, is low enough to be neglected, as indicated by the XRD and EDS results (see **Figure 4-5** and **Figure 4-10**). Thus, in the process of oxidation, $Al_2O_3$ and $Cr_2O_3$ performed as a pair of competing oxides, and their competition is the core mechanism of the oxide formation. To explain the mechanism of competing oxide formation in CoNiCrAl alloy, normally 4 factors, free energies of formation, the atomic ratio, the rate constants for the formation, and the inter-diffusion coefficient of two elements are considered [76]. Rate constant for the formation is simply a molar ratio between reactants in a reaction, and large rate constant normally result in low priority of oxidation. As long as they are both 1.5 for oxidation of $Al_2O_3$ and $Cr_2O_3$ in this study, the impact of this factor can be ignored. A high inter-diffusion rate of an element ensures that a sufficient amount of it is available on the surface for oxidation. Consequently, higher inter-diffusion can lead to an increased reaction rate. In the following section, the inter-diffusion coefficient is used to calculate exclusive oxide growth.

From theoretical value of free energy of oxide formation, $0 > \Delta G_\theta(Cr_2O_3) > \Delta G_\theta(Al_2O_3)$.For the reason of Al's high negative free energy of formation, it is easier to be oxidised than most of metal elements in the early stage of oxidation, such as Cr in this study. Moreover, its product of oxidation has a higher thermodynamic stability than oxides of other metal elements. In early stage of oxidation, for the influential role of free energy of formation, Al in alloys of low Cr-to-Al ratio experienced a selective oxidation for its high free energy of formation. Consequently, exclusive $Al_2O_3$ layer can be found in alloys at ratios of 0.3-1.8.

In the later stage of oxidation, the role of atomic ratio becomes crucial in oxidation process. It can be proved by the microstructure evolution in the alloy at ratio of 1.8, where $Al_2O_3$ is formed earlier than $Cr_2O_3$. There was no dual layer of $Cr_2O_3$ and $Al_2O_3$ can be found in cross-section view of the alloy at ratio of 1.8 (see **Figure 4-7**(d)), nor $Cr_2O_3$ can be found in surface morphology after just 2 h oxidation (see **Figure 4-6**(j)). In contrast, no dense layer of $Al_2O_3$ can be found in cross-section view of the ratio 1.8 alloy (see **Figure 4-8**(d)), and few of $Al_2O_3$ can be found in surface morphology after 100 h oxidation (see **Figure 4-6**(l)). It can be inferred that in the alloys at high Cr-to-Al ratio, layer of $Al_2O_3$ is the transition pattern of the dual layer of $Cr_2O_3$ and $Al_2O_3$, formed before Al content, or β phase, depleted by the formation of alumina layer. In low ratio samples, γ phase (Cr rich) was isolated from the air by the intact $Al_2O_3$ layer, thus the formation of $Cr_2O_3$ is prevented. Formation of dense $Al_2O_3$ layer was hindered in oxidation process of the alloys at ratio of 2.8 by its insufficient Al content, or it possibly can be found in initial stage of the oxidation process.

High Cr content could reduce the coverage of alumina and form an additional layer of $Cr_2O_3$ on top of $Al_2O_3$ [77]. Ratio 1.8 is the threshold which certifies if chromium can infiltrate the layer of alumina and be able to form a separate layer of chromium oxide on top of alumina layer. The β phase distribution in the alloy at ratio of 1.8 is considered to be explanation of the co-existence of dense $Al_2O_3$ layer, and dual-layer of $Cr_2O_3$ and $Al_2O_3$. As long as β phase is rare in ratio 1.8 alloy, a continuous protective alumina scale is not attainable to be formed to prevent out diffusion by high concentration of Cr. Instead, corresponding pieces of alumina layer were formed above the β-rich regions. Therefore, Cr is allowed to diffuse through cracks to the surface forming an extra oxide layer of $Cr_2O_3$, above the $Al_2O_3$ layer.

Though presence of aluminium nitride beneath the $Al_2O_3$ layer is primarily attributed to the less dense property of chromium oxide compared to alumina, dual layer of $Al_2O_3$ and $Cr_2O_3$ can reduces oxide growth rate of O inward transport and improves scale adhesion [78]. Consequently, while the presence of chromium reduces high-temperature corrosion, the alloys at a higher Cr-to-Al ratio exhibit greater AlN content.

### 4.6 Threshold of $Cr_2O_3$ formation

It was shown that the oxidation evolution of CoNiCrAl is mainly consisted by the formation of dense α-$Al_2O_3$ scale in β phase rich regions in alloys of low Cr-to-Al ratio, and formation of dual layer of $Cr_2O_3$ and $Al_2O_3$ in γ-phase rich regions in alloys of high Cr-to-Al ratio, and both appeared in alloys of 1.8 Cr-to-Al ratio. The threshold of formation of $Cr_2O_3$ is not remained constant during oxidation evolution. It can be inferred from **Figure 4-7**(e), in the early stage of oxidation, the oxidation of Al is favoured for its high free energy of formation, thus $Cr_2O_3$ cannot be found in the alloy of ratio 1.8.In later stage of oxidation, due to the Al depletion region, the growth of $Al_2O_3$ cannot be maintained. Therefore, the threshold of $Cr_2O_3$ formation is reduced.

Wagnar theory can be referenced to predict the threshold theoretically [79]. The theory is primarily used to predict the minimum concentration required for a solute to form exclusive oxide. If a continuous $Al_2O_3$ scale is allowed to be formed, a minimum threshold for Al concentration is required to facilitate an exclusive growth of $Al_2O_3$ and isolate the reactive air avoiding formation of other oxide. Wagnar theory can be expressed as following:

$$N_{Al}^{(1)} \geq [f(\frac{V_m}{V_{ox}})\pi \frac{N_O^S D_O}{2\nu D_{Al}}]^{\frac{1}{2}} \quad (4.1)$$

$N_{Al}^{(1)}$ is the lower threshold of Al concentration (atomic percentage) in this study to form

exclusive $Al_2O_3$ layer, $f$ is the volume fraction of internal oxide, $V_m$and $V_{ox}$ are the respective molar volumes of the alloy and oxide, $N_O^S$ is the solubility of oxygen in the alloy (atomic percentage), $D_O$ is the diffusivity of oxygen in the alloy, $\nu$ is the stoichiometric ratio of oxygen to Al in $Al_2O_3$, which is 1.5, and $D_{Al}$ is the diffusion coefficient of the Al in the alloy.

The theoretical $N_{Al}^{(1)}$ can be derived from the parameters estimated in **Table 4-2** using the calculations from **Eq. (4.1)**, which is 9.17%. The experimental result, the Al percentage of ratio 1.8 is 6.5%, which is lower than the theoretical prediction. Though the atomic percentage of Al of the experimental can be lower than the threshold, the existence of β phase, which has approximately 35% atomic percentage of Al, as an "Al-reservoir", provides sufficient Al to form dense $Al_2O_3$ layer. Moreover, $Al_2O_3$ layer can form above the β phase even in alloys of high Cr-to-Al ratio, but hard to be noticed in early stage by morphology. As composition change in phases is not significant by Cr-to-Al ratio variation, proportion of phases should be responsible for the transformation of oxide layer formation.

**Table 4-2** Parameters for estimation of exclusive $Al_2O_3$ formation in the CoNiCrAl alloys at Cr-to-Al ratio of 1.8.

| Parameter | Value | Unit |
|---|---|---|
| $V_m$ | $7.184 \times 10^{-6}$ | $m^3/mol$ |
| $V_{ox}$ | $25.575 \times 10^{-6}$ | $m^3/mol$ |
| $f$ | 34 | % |
| $N_O^S$ | 0.001 [80] | |
| $D_O$ | $10^{-12}$ [81] | $m^2/s$ |
| $D_{Al}$ | $1.19 \times 10^{-14}$ [82] | $m^2/s$ |

Secondly, to explore reduction of the threshold, an additional method is derived to predict the threshold of maintaining [76]:

$$N_{Al}^{(2)} \geq \frac{V_m}{2\nu M_O} \left[\frac{\pi k_p}{D_{Al}}\right]^{\frac{1}{2}} \quad (4.2)$$

$N_{Al}^{(2)}$ is the threshold of Al concentration (atomic percentage) in this study to maintain the external scale formation, $k_p$ is the rate for continuous oxide scale growth ($g^2/m^4s$), and $M_O$ is the molar mass of the oxidant. Similar to **Eq. (4.1)**, $D_{Al}$ represents the diffusion coefficient of Al and $V_m$ represents the molar volumes of the alloy in **Eq. (4.2)**.

The theoretical $N_{Al}^{(2)}$ can be derived from the parameters estimated in **Table 4-3** using the calculations from **Eq. (4.2)**, which only 3.33 atomic percent of Al is required for maintaining an external scale formation. However, in the alloy of 1.8 Cr-to-Al ratio, exclusive alumina $Al_2O_3$ is failed to be maintained. Though $N_{Al}^{(2)}$ is significantly lower than $N_{Al}^{(1)}$, the extraction of Al in early stage of oxidation drops the concentration of Al to an extremely low level forming an Al depletion region beneath the $Al_2O_3$ layer and leads to the failure of maintaining exclusive $Al_2O_3$ layer.

**Table 4-3** Parameters for estimation of maintaining external scale formation in the CoNiCrAl alloys at Cr-to-Al ratio of 1.8.

| Parameter | Value | Unit |
|---|---|---|
| $V_m$ | $7.184\times 10^{-6}$ | $m^3/mol$ |
| $M_O$ | 16 | g/mol |
| $k_p$ | $1.88\times10^{-4}$ [83] | $g^2/m^4/s$ |
| $D_{Al}$ | $1.19 \times 10^{-14}$ | $m^2/s$ |

After 100 h oxidation, sufficient Cr diffuses to the surface of the alloys of low Cr-to-Al ratio

to form $Cr_2O_3$ layer on surface. The structure of alloys at ratio 1.8 is then stabilised to be covered by $Cr_2O_3$ and $Al_2O_3$ layers. For alloys of low Cr-to-Al ratio, an intact $Al_2O_3$ layer forms before Al was depleted beneath, preventing the formation of other oxides maintaining an exclusive dense $Al_2O_3$ layer.

# Chapter 5 Conclusion

In this study, the effects of Cr-to-Al ratio on microstructure evolution and oxidation mechanism of as-cast CoNiCrAl alloys prepared by VAM method were investigated after heat treatment. The microstructure and oxidation characteristics of the CoNiCrAl alloys at five different ratios, 0.3, 0.8, 1.3, 1.8 and 2.8, were analysed to reveal the oxide growth mechanisms at different Cr-to-Al ratios. The conclusions are drawn as follows:

- Dense $Al_2O_3$ layer formed by selective oxidation is the main oxidation mechanism in CoNiCrAl alloys of low Cr-to-Al ratio, and formation of $Cr_2O_3$, an outer layer grows on the $Al_2O_3$ layer, as a substitute oxide especially in γ-phase rich alloys of high Cr-to-Al ratio. Both oxides appear at the threshold of $Cr_2O_3$ formation, approximately at a Cr-to-Al ratio of 1.8, which significantly influences the oxidation resistance and path of O and N diffusion by distinct structures of oxide layer.
- The experimental Cr-to-Al ratio threshold for Al exclusive formation is lower than the theoretical value. This discrepancy is primarily due to the presence of β phase, which serves as an "Al reservoir" with an approximate atomic percentage of 35% Al. However,

maintaining of the exclusive $Al_2O_3$ layer can fail due to the extraction of Al during the early stage of oxidation, which significantly reduces the Al concentration and creates an Al depletion region beneath the $Al_2O_3$ layer.

- As the oxidation time increases, due to the Al depletion region formed by initial Al extraction, the atomic ratio of Al decreases, and the growth of exclusive $Al_2O_3$ layers cannot be maintained, indicating that the threshold of Cr-to-Al is reduced. Therefore, for the studied CoNiCrAl alloys, formation of $Cr_2O_3$ is favoured in long term and formation of $Al_2O_3$ is favoured in short term.

# Chapter 6 Future work

This thesis primarily focuses on the effects of Cr-to-Al ratio on the oxidation behaviour of CoNiCrAl alloys. A significant threshold of 1.8 for Cr-to-Al ratio was identified as a critical factor influencing the formation of $Cr_2O_3$ and AlN. However, this study has certain limitations: the proportions of Ni and Co were kept constant; heat treatment was assessed qualitatively rather than quantitatively; the focus was solely on microstructure evolution, without exploring the oxidation resistance and the mechanical strength due to sampling constraints and time limitations; and the composition of the CoNiCrAl alloy serves only as a simplified model of MCrAlY alloys for foundational mechanism exploration without any additives.

Future research can be expanded on following topics in several ways:

- Effects of Al proportion: the effects of varying the Al content in low Al content CoNiCrAl alloys on the oxidation behaviour will be inspected. By keeping the relative proportions of Co, Ni, and Cr constant, the potential impact of Al can be explored further, especially since high Al content effects have already been studied [69]. This investigation may also reveal the roles of Co and Ni in influencing the Cr-to-Al ratio threshold for $Cr_2O_3$ formation.
- Pt addition studies: the effects of Pt additive on the oxidation behaviour of CoNiCrAl bond coat alloy will be examined. Previous studies suggest that addition of Pt can enhances cohesion of CoNiCrAl alloy and reduces oxidation rates when added as an extra separate bond coat layer, thereby limiting inner diffusion to the substrate [84]. A future work of direct addition of Pt as an alloying element to modify the microstructure of

CoNiCrAl alloy, enabling tracking of oxidation evolution and analysis of Pt's role in enhancing oxidation resistance. Subsequent investigations will include microstructure analysis, phase equilibria calculations, and evaluations of oxidation resistance to assess the effectiveness of Pt in the MCrAlY alloy system.

- Heat treatment studies: various heat treatment methods applied to the CoNiCrAl alloys prior to oxidation tests will be explored to determine their effects on phase homogeneity, transformation, and overall performance of MCrAlY alloys. This study will help assess whether heat treatment processes can be simplified or even omitted to reduce costs without compromising performance.
- Mechanical strength examination: mechanical tests will be conducted on the oxidised CoNiCrAl alloys to study if formation of extra $Cr_2O_3$ and AlN during the oxidation of high Cr content CoNiCrAl alloys can result in enhanced mechanical strength of CoNiCrAl alloys. This investigation will help to clarify the relationship between oxidation processes and mechanical properties.

# References


[1] G.W. Goward, Progress in coatings for gas turbine airfoils, Surf Coating Technol 108 (1998) 73–79. https://doi.org/10.1016/S0257-8972(98)00667-7

[2] N.J.S. J.R. Nicholls, W.Y. Chan, H.E. Evans, Smart overlay coatings — concept and practice, Surf Coating Technol 149 (2002) 236-244. https://doi.org/10.1016/S0257-8972(01)01499-2

[3] F. Ghadami, A. Sabour Rouh Aghdam, S. Ghadami, Microstructural characteristics and oxidation behavior of the modified MCrAlX coatings: A critical review, Vacuum 185 (2021) 109980. https://doi.org/10.1016/j.vacuum.2020.109980

[4] N.P. Padture MG, E.H. Jordan, Thermal barrier coatings for gas-turbine engine applications, Science 296 (2002) 280-284. https://doi.org/10.1126/science.1068609

[5] W.G. Sloof, T.J. Nijdam, On the high-temperature oxidation of MCrAlY coatings, Int J Mater Res 100 (2009) 1318-1330. https://doi.org/doi:10.3139/146.110201

[6] D. Naumenko, V. Shemet, L. Singheiser, W.J. Quadakkers, Failure mechanisms of thermal barrier coatings on MCrAlY-type bondcoats associated with the formation of the thermally grown oxide, J Mater Sci 44 (2009) 1687-1703. https://doi.org/10.1007/s10853-009-3284-3

[7] T.J. Nijdam, W.G. Sloof, Microstructural evolution of a MCrAlY coating upon isothermal annealing, Mater Charact 59 (2008) 1697-1704. https://doi.org/10.1016/j.matchar.2008.03.011

[8] I. Gurrappa, Identification of hot corrosion resistant MCrAlY based bond, Surf Coating Technol 139 (2001) 272-283. https://doi.org/10.1016/S0257-8972(00)01156-7

[9] X. Zhan, D. Wang, Z. Ge, Y. Zhang, J. Dong, L. Lou, J. Zhang, Microstructural evolution of NiCoCrAlY coated directionally solidified superalloy, Surf Coating Tech 440 (2022) 128487. https://doi.org/https://doi.org/10.1016/j.surfcoat.2022.128487

[10] H. Chen, Microstructure characterisation of un-melted particles in a plasma sprayed CoNiCrAlY coating, Mater Charact 136 (2018) 444-451. https://doi.org/10.1016/j.matchar.2017.09.020

[11] L. Li, Y. Chen, A. Huang, X. Liu, H. Zhang, H. Zhang, X. Zhang, J. Lu, X. Zhao, A novel NiCoCrAlPt high-entropy alloy with superb oxidation resistance at 1200 °C, Corros Sci 228 (2024) 111819. https://doi.org/10.1016/j.corsci.2024.111819

[12] R. Eriksson, K. Yuan, X.-H. Li, R. Lin Peng, MCrAlY coating design based on oxidation–diffusion modelling. Part II: Lifing aspects, Surf Coating Technol 253 (2014) 27-37. https://doi.org/10.1016/j.surfcoat.2014.05.010

[13] D. Texier, D. Monceau, S. Selezneff, A. Longuet, E. Andrieu, High Temperature Micromechanical Behavior of a Pt-Modified Nickel Aluminide Bond-Coating and of Its Interdiffusion Zone with the Superalloy Substrate, Metall Mater Trans A 51 (2020) 1475-1480. https://doi.org/10.1007/s11661-020-05634-2

[14] D.B. Miracle, O.N. Senkov, A critical review of high entropy alloys and related concepts, Acta Mater 122 (2017) 448-511. https://doi.org/10.1016/j.actamat.2016.08.081

[15] Y. Itoh, M. Saitoh, Mechanical Properties of Overaluminized MCrAlY Coatings at Room Temperature, J Eng Gas Turbine Power 127 (2005) 807-813. https://doi.org/10.1115/1.1688766

[16] R.D. Noebe, FJ. Ritzert, A. Misra, R. Gibala, Prospects for Ductility and Toughness Enhancement of Nial by Ductile Phase Reinforcement, (1991).

[17] E.J. Pickering, N.G. Jones, High-entropy alloys: a critical assessment of their founding principles and future prospects, Int Mater Rev 61 (2016) 183-202. https://doi.org/10.1080/09506608.2016.1180020

[18] D. Salehi Doolabi, M.R. Rahimipour, M. Alizadeh, S. Pouladi, S.M.M. Hadavi, M.R. Vaezi, Effect of high vacuum heat treatment on microstructure and cyclic oxidation resistance of HVOF-CoNiCrAlY coatings, Vacuum

135 (2017) 22-33. https://doi.org/10.1016/j.vacuum.2016.10.014
[19] H. Chen, Z. Li, L. Li, H. Guo, A. Rushworth, X. Wang, Microstructure evolution of as-cast CoNiCrAl bond coat alloys after isothermal heat treatments, Mater Charact 204 (2023) 113183. https://doi.org/10.1016/j.matchar.2023.113183
[20] C. Schneider, Rasband, W. & Eliceiri, K, NIH Image to ImageJ: 25 years of image analysis, Nat Methods 9 (2012) 671-675. https://doi.org/10.1038/nmeth.2089
[21] R. Darolia, Thermal barrier coatings technology: critical review, progress update, remaining challenges and prospects, Int Mater Rev 58 (2013) 315-348. https://doi.org/10.1179/1743280413Y.0000000019
[22] D.K. Das, Microstructure and high temperature oxidation behavior of Pt-modified aluminide bond coats on Ni-base superalloys, Progress in Materials Science 58 (2013) 151-182. https://doi.org/https://doi.org/10.1016/j.pmatsci.2012.08.002
[23] J.A. Haynes, M. Ferber, W. Porter, Thermal cycling behavior of plasma-sprayed thermal barrier coatings with various MCrAlX bond coats, J Therm Spray Technol 9 (2000) 38-48. https://doi.org/10.1361/105996300770350041
[24] J.-W. Yeh, S.-K. Chen, S.-J. Lin, J.-Y. Gan, T.-S. Chin, T.-T. Shun, C.-H. Tsau, S.-Y. Chang, Nanostructured High-Entropy Alloys with Multiple Principal Elements: Novel Alloy Design Concepts and Outcomes, Adv Eng Mater 6 (2004) 299-303. https://doi.org/10.1002/adem.200300567
[25] J.-l. Zhou, Y.-h. Cheng, Y.-x. Chen, X.-b. Liang, Composition design and preparation process of refractory high-entropy alloys: A review, Int J Refract Hard Met 105 (2022). https://doi.org/10.1016/j.ijrmhm.2022.105836
[26] N.F. Lone, F. Czerwinski, D. Chen, Present challenges in development of lightweight high entropy alloys: A review, Appl Mater Today 39 (2024) 102296. https://doi.org/10.1016/j.apmt.2024.102296
[27] S.S. S.S. Nene, D.K. Yadav, A. Dutta,, Metallurgical aspects of high entropy alloys, J Alloys Compd 1005 (2024) 175849. https://doi.org/10.1016/j.jallcom.2024.175849.
[28] K. Li, W. Chen, Recent progress in high-entropy alloys for catalysts: synthesis, applications, and prospects, Mater Today Energy 20 (2021) 100638. https://doi.org/10.1016/j.mtener.2021.100638
[29] Y.F. Ye, Q. Wang, J. Lu, C.T. Liu, Y. Yang, High-entropy alloy: challenges and prospects, Mater Today 19 (2016) 349-362. https://doi.org/10.1016/j.mattod.2015.11.026
[30] Z. Cui, Y. Mi, D. Qiu, P. Dong, Z. Qin, D. Gong, W. Li, Microstructure and mechanical properties of additively manufactured CrMnFeCoNi high-entropy alloys after ultrasonic surface rolling process, J Alloys Compd 887 (2021) 161393. https://doi.org/10.1016/j.jallcom.2021.161393
[31] Z. Wu, H. Bei, G.M. Pharr, E.P. George, Temperature dependence of the mechanical properties of equiatomic solid solution alloys with face-centered cubic crystal structures, Acta Mater 81 (2014) 428-441. https://doi.org/10.1016/j.actamat.2014.08.026
[32] C. Varvenne, A. Luque, W.A. Curtin, Theory of strengthening in fcc high entropy alloys, Acta Mater 118 (2016) 164-176. https://doi.org/10.1016/j.actamat.2016.07.040
[33] K.Y. Tsai, M.H. Tsai, J.W. Yeh, Sluggish diffusion in Co–Cr–Fe–Mn–Ni high-entropy alloys, Acta Mater 61 (2013) 4887-4897. https://doi.org/10.1016/j.actamat.2013.04.058
[34] M.-H. Tsai, J.-W. Yeh, J.-Y. Gan, Diffusion barrier properties of AlMoNbSiTaTiVZr high-entropy alloy layer between copper and silicon, Thin Solid Films 516 (2008) 5527-5530. https://doi.org/10.1016/j.tsf.2007.07.109
[35] J. Dąbrowa, M. Zajusz, W. Kucza, G. Cieślak, K. Berent, T. Czeppe, T. Kulik, M. Danielewski, Demystifying the sluggish diffusion effect in high entropy alloys, J Alloys Compd 783 (2019) 193-207. https://doi.org/10.1016/j.jallcom.2018.12.300
[36] E.P. George, Raabe, D. & Ritchie, R.O., High-entropy alloys, Nat Rev Mater 4 (2019) 515–534.

https://doi.org/10.1038/s41578-019-0121-4
[37] B.S. Murty, J.W. Yeh, S. Ranganathan, P.P. Bhattacharjee, High-entropy alloys, Elsevier2019. https://doi.org/10.1016/C2017-0-03317-7
[38] Y. Wang, Y. Wang, High-entropy alloys in catalyses and supercapacitors: Progress, prospects, Nano Energy 104 (2022). https://doi.org/10.1016/j.nanoen.2022.107958
[39] D.R.G. Achar, R. Munoz-Arroyo, L. Singheiser, W.J. Quadakkers, Modelling of phase equilibria in MCrAlY coating systems, Surf Coating Tech 187 (2004) 272-283. https://doi.org/https://doi.org/10.1016/j.surfcoat.2004.02.018
[40] J. Chen, X. Zhou, W. Wang, B. Liu, Y. Lv, W. Yang, D. Xu, Y. Liu, A review on fundamental of high entropy alloys with promising high–temperature properties, J Alloys Compd 760 (2018) 15-30. https://doi.org/10.1016/j.jallcom.2018.05.067
[41] J. Zhu, S. Lu, Y. Jin, L. Xu, X. Xu, C. Yin, Y. Jia, High-Temperature Oxidation Behaviours of AlCoCrFeNi High-Entropy Alloy at 1073–1273 K, Oxid Met 94 (2020) 265-281. https://doi.org/10.1007/s11085-020-09991-6
[42] K. Ogawa, High temperature oxidation behavior of thermal barrier coatings, Materials, Modeling and Performance (2015) 103-127. https://doi.org/10.5772/59794
[43] E. Serrano Perez, H. Martinez Gutierrez, F. Juarez Lopez, Corrosion of MCrAlY: Pt composites prepared by spark plasma sintering, Corros Eng Sci Technol 53 (2018) 539-548. https://doi.org/10.1080/1478422x.2018.1511314
[44] O. Kazuhiro, High Temperature Oxidation Behavior of Thermal Barrier Coatings, in: I. Gurrappa (Ed.), Gas Turbines, IntechOpen, Rijeka, 2015, pp. Ch. 4.
[45] F.J. Pennisi, D.K. Gupta, Improved plasma-sprayed Ni-Co-Cr-Al-Y and Co-Cr-Al-Y coatings for aircraft gas turbine applications, Thin Solid Films 84 (1981) 49-58. https://doi.org/10.1016/0040-6090(81)90009-2.
[46] R. Lowrie, D.H. Boone, Composite coatings of CoCrAlY plus platinum, Thin Solid Films 45 (1977) 491-498. https://doi.org/10.1016/0040-6090(77)90236-X.
[47] D. Guo, L. Zhao, B. Jodoin, Cold spray for production of in-situ nanocrystalline MCrAlY coatings – Part II: Isothermal oxidation performance, Surf Coating Tech 409 (2021) 126828. https://doi.org/https://doi.org/10.1016/j.surfcoat.2021.126828
[48] Y. Itoh, M. Saitoh, K. Takaki, K. Fujiyama, Effect of high-temperature protective coatings on fatigue lives of nickel-based superalloys, Fatigue & Fracture of Engineering Materials & Structures 24 (2001) 843-854.
[49] H. Chen, A. Rushworth, Effects of oxide stringers on the β-phase depletion behaviour in thermally sprayed CoNiCrAlY coatings during isothermal oxidation, J. Mater. Sci. Technol. 45 (2020) 108-116. https://doi.org/https://doi.org/10.1016/j.jmst.2019.11.018
[50] Neil Birks, Gerald H. Meier, F.S. Pettit, Introduction to the high temperature oxidation of metals, second ed., Cambridge University Press, 2006. https://doi.org/10.1017/CBO9781139163903
[51] C. Chen, J. Zhang, C. Duan, X. Feng, Y. Shen, Investigation of Cr–Al composite coatings fabricated on pure Ti substrate via mechanical alloying method: Effects of Cr–Al ratio and milling time on coating, and oxidation behavior of coating, J Alloys Compd 660 (2016) 208-219. https://doi.org/10.1016/j.jallcom.2015.11.094
[52] Z.R. Liu, J. Zhang, X. Sun, J.W. Du, S.Q. Wang, L. Chen, Microstructure, mechanical properties, and oxidation behavior of arc-evaporated Cr–Al–O–N coatings with various Cr/Al ratios, Ceram Int 49 (2023) 16412-16421. https://doi.org/10.1016/j.ceramint.2023.02.002
[53] S. Zeng, P. Li, J. Tian, C. Chen, Y. Meng, C. Zhu, H. Shen, X. Han, H. Zhang, Influence of Al content on the oxidation behavior of CrAl coating on Zry-4 alloys in 1200 °C steam, Corros Sci 198 (2022) 110115. https://doi.org/https://doi.org/10.1016/j.corsci.2022.110115
[54] M. Pohler, R. Franz, J. Ramm, P. Polcik, C. Mitterer, Seed layer stimulated growth of crystalline high Al

containing (Al,Cr)2O3 coatings deposited by cathodic arc evaporation, Thin Solid Films 550 (2014) 95-104. https://doi.org/10.1016/j.tsf.2013.10.125

[55] S. Arun, N. Radhika, B. Saleh, Advances in vacuum arc melting for high entropy alloys: A review, Vacuum 226 (2024). https://doi.org/10.1016/j.vacuum.2024.113314

[56] Y. Lv, R. Hu, Z. Yao, J. Chen, D. Xu, Y. Liu, X. Fan, Cooling rate effect on microstructure and mechanical properties of Al x CoCrFeNi high entropy alloys, Mater Des 132 (2017) 392-399. https://doi.org/10.1016/j.matdes.2017.07.008

[57] Y. Zhang, S.G. Ma, J.W. Qiao, Morphology Transition from Dendrites to Equiaxed Grains for AlCoCrFeNi High-Entropy Alloys by Copper Mold Casting and Bridgman Solidification, Metall Mater Trans A 43 (2011) 2625-2630. https://doi.org/10.1007/s11661-011-0981-8

[58] L.J. Santodonato, Y. Zhang, M. Feygenson, C.M. Parish, M.C. Gao, R.J. Weber, J.C. Neuefeind, Z. Tang, P.K. Liaw, Deviation from high-entropy configurations in the atomic distributions of a multi-principal-element alloy, Nat Commun 6 (2015) 5964. https://doi.org/10.1038/ncomms6964

[59] S. Ragunath, N. Radhika, S. Aravind Krishna, N. Jeyaprakash, Enhancing microstructural, mechanical and tribological behaviour of AlSiBeTiV high entropy alloy reinforced SS410 through friction stir processing, Tribol Int 188 (2023). https://doi.org/10.1016/j.triboint.2023.108840

[60] Y.P. Wang, B.S. Li, M.X. Ren, C. Yang, H.Z. Fu, Microstructure and compressive properties of AlCrFeCoNi high entropy alloy, Mater Sci Eng A 491 (2008) 154-158. https://doi.org/10.1016/j.msea.2008.01.064

[61] K.B. Zhang, Z.Y. Fu, J.Y. Zhang, J. Shi, W.M. Wang, H. Wang, Y.C. Wang, Q.J. Zhang, Annealing on the structure and properties evolution of the CoCrFeNiCuAl high-entropy alloy, J Alloys Compd 502 (2010) 295-299. https://doi.org/10.1016/j.jallcom.2009.11.104

[62] K.R. Lim, K.S. Lee, J.S. Lee, J.Y. Kim, H.J. Chang, Y.S. Na, Dual-phase high-entropy alloys for high-temperature structural applications, J Alloys Compd 728 (2017) 1235-1238. https://doi.org/10.1016/j.jallcom.2017.09.089

[63] J. Cieslak, J. Tobola, J. Przewoznik, K. Berent, U. Dahlborg, J. Cornide, S. Mehraban, N. Lavery, M. Calvo-Dahlborg, Multi-phase nature of sintered vs. arc-melted CrxAlFeCoNi high entropy alloys - experimental and theoretical study, J Alloys Compd 801 (2019) 511-519. https://doi.org/10.1016/j.jallcom.2019.06.121

[64] I. Keller, D. Naumenko, W.J. Quadakkers, R. Vaßen, L. Singheiser, Influence of vacuum heat treatment parameters on the surface composition of MCrAlY coatings, Surf Coating Technol 215 (2013) 24-29. https://doi.org/10.1016/j.surfcoat.2012.09.066

[65] Y.-O. Jung, M.-S. Kim, J. Park, G. Yang, D.W. Lee, S.-W. Kim, Achieving fine fully lamellar microstructure of casting TiAl alloy by simple heat treatment, Mater Charact 200 (2023) 112881. https://doi.org/10.1016/j.matchar.2023.112881

[66] J. Lu, H. Zhang, Y. Chen, L. Li, X. Liu, W. Xiao, N. Ni, X. Zhao, F. Guo, P. Xiao, Y-doped AlCoCrFeNi2.1 eutectic high-entropy alloy with excellent oxidation resistance and structure stability at 1000°C and 1100°C, Corros Sci 180 (2021) 109191. https://doi.org/https://doi.org/10.1016/j.corsci.2020.109191

[67] G.-H. Meng, B.-Y. Zhang, H. Liu, G.-J. Yang, T. Xu, C.-X. Li, C.-J. Li, Vacuum heat treatment mechanisms promoting the adhesion strength of thermally sprayed metallic coatings, Surf Coating Technol 344 (2018) 102-110. https://doi.org/10.1016/j.surfcoat.2018.03.010

[68] G.-H. Meng, H. Liu, M.-J. Liu, T. Xu, G.-J. Yang, C.-X. Li, C.-J. Li, Highly oxidation resistant MCrAlY bond coats prepared by heat treatment under low oxygen content, Surf Coating Technol 368 (2019) 192-201. https://doi.org/10.1016/j.surfcoat.2019.04.046

[69] A. Huang, Y. Chen, Z. Zhang, J. Shen, L. Li, X. Liu, H. Zhang, J. Lu, X. Zhao, Effect of Al content on the oxidation behavior of NiCoCrAlYHf alloys at 1100 ℃, Corros Sci 222 (2023) 111417.

https://doi.org/10.1016/j.corsci.2023.111417
[70] P. Lyu, Q. Gao, X. You, T. Peng, H. Yuan, Q. Guan, J. Cai, H. Liu, X. Liu, C. Zhang, High temperature oxidation enhanced by laser remelted of CoCrFeNiAlx (x = 0.1, 0.5 and 1) high-entropy alloys, J Alloy Compd 915 (2022) 165297. https://doi.org/https://doi.org/10.1016/j.jallcom.2022.165297
[71] A. Mohanty, J.K. Sampreeth, O. Bembalge, J.Y. Hascoet, S. Marya, R.J. Immanuel, S.K. Panigrahi, High temperature oxidation study of direct laser deposited AlXCoCrFeNi (X=0.3,0.7) high entropy alloys, Surf Coating Tech 380 (2019) 125028. https://doi.org/10.1016/j.surfcoat.2019.125028
[72] C. Zhu, P. Li, C. Chen, J. Tian, S. Zeng, Y. Meng, H. Shen, X. Han, H. Zhang, Microstructure evolution and oxidation behavior of bi-layer CrAl-Mo coated Zircaloy-4 in steam at 1200 °C and 1300 °C, Corros Sci 208 (2022) 110632. https://doi.org/https://doi.org/10.1016/j.corsci.2022.110632
[73] S. Zeng, C. Chen, M. Li, L. Qi, Y. Meng, C. Zhu, X. Han, H. Zhang, Aluminum concentration effect on the oxidation behavior of CrAl coatings investigated by high-throughput method, Corros Sci 221 (2023) 111327. https://doi.org/https://doi.org/10.1016/j.corsci.2023.111327
[74] T. Zhang, D.Y. Li, Effects of yttrium on corrosive erosion and dry sand erosion of FeAlCr(Y) diffusion coatings on 1030 steel, Metall Mater Trans A 277 (2000) 18-24. https://doi.org/https://doi.org/10.1016/S0921-5093(99)00559-6
[75] J.G. Smeggil, Some comments on the role of yttrium in protective oxide scale adherence, Mater Sci Eng 87 (1987) 261-265. https://doi.org/https://doi.org/10.1016/0025-5416(87)90387-9
[76] C. Wagner, Theoretical analysis of the diffusion processes determining the oxidation rate of alloys, J Electrochem Soc 99 (1952) 369. https://doi.org/10.1149/1.2779605
[77] A. Mohanty, J.K. Sampreeth, O. Bembalge, J.Y. Hascoet, S. Marya, R.J. Immanuel, S.K. Panigrahi, High temperature oxidation study of direct laser deposited AlXCoCrFeNi (X=0.3,0.7) high entropy alloys, Surf Coating Technol 380 (2019) 125028. https://doi.org/10.1016/j.surfcoat.2019.125028
[78] B.A. Pint, Experimental observations in support of the dynamic-segregation theory to explain the reactive-element effect, Oxid Met 45 (1996) 1–37. https://doi.org/10.1007/BF01046818
[79] C. Wagner, Reaktionstypen bei der Oxydation von Legierungen, Zeitschrift für Elektrochemie, Berichte der Bunsengesellschaft für physikalische Chemie 63 (1959) 772-782.
[80] S.W. Guan, W.W. Smeltzer, Oxygen solubility and a criterion for the transition from internal to external oxidation of ternary alloys, Oxid Met 42 (1994) 375-391. https://doi.org/10.1007/BF01046756
[81] A.J. Ross, H.Z. Fang, S.L. Shang, G. Lindwall, Z.K. Liu, A curved pathway for oxygen interstitial diffusion in aluminum, Comput Mater Sci 140 (2017) 47-54. https://doi.org/10.1016/j.commatsci.2017.08.014
[82] M.S.A. Karunaratne, S.L. Ogden, S.D. Kenny, R.C. Thomson, A multicomponent diffusion model for prediction of microstructural evolution in coated Ni based superalloy systems, Mater Sci Technol 25 (2009) 287-299. https://doi.org/10.1179/174328408X355415
[83] G. Geramifard, C. Schulz, P. Franke, H. Seifert, Oxidation behaviour of NiAl intermetallics with embedded Cr and Mo, Corros Sci 177 (2020) 108956. https://doi.org/10.1016/j.corsci.2020.108956
[84] H. Xiao, J. Sun, W. Li, S. Jiang, Effect of Pt modification on hot corrosion resistance of NiCrAlYSi+AlY coating at 900 ℃, Mater Today Commun 34 (2023) 105366. https://doi.org/10.1016/j.mtcomm.2023.105366